



LUND UNIVERSITY

Improved Cloud Parameterization in Global Climate Model

Aerosol effects and secondary ice production mechanisms

Jadav, Arti

2024

[Link to publication](#)

Citation for published version (APA):

Jadav, A. (2024). *Improved Cloud Parameterization in Global Climate Model: Aerosol effects and secondary ice production mechanisms*. [Doctoral Thesis (compilation), Dept of Physical Geography and Ecosystem Science]. Lund University.

Total number of authors:

1

General rights

Unless other specific re-use rights are stated the following general rights apply:

Copyright and moral rights for the publications made accessible in the public portal are retained by the authors and/or other copyright owners and it is a condition of accessing publications that users recognise and abide by the legal requirements associated with these rights.

- Users may download and print one copy of any publication from the public portal for the purpose of private study or research.
- You may not further distribute the material or use it for any profit-making activity or commercial gain
- You may freely distribute the URL identifying the publication in the public portal


Read more about Creative commons licenses: <https://creativecommons.org/licenses/>

Take down policy

If you believe that this document breaches copyright please contact us providing details, and we will remove access to the work immediately and investigate your claim.

LUND UNIVERSITY

PO Box 117
221 00 Lund
+46 46-222 00 00



Improved Cloud Parameterization in Global Climate Model: Aerosol effects and secondary ice production mechanisms

ARTI JADAV

DEPARTMENT OF PHYSICAL GEOGRAPHY AND ECOSYSTEM SCIENCE | LUND UNIVERSITY





Department of Physical Geography
and Ecosystem Science
Faculty of Science

ISBN 978-91-89187-37-5

Improved Cloud Parameterization in Global Climate Model:
Aerosol effects and secondary ice production mechanisms

Improved Cloud Parameterization in Global Climate Model: Aerosol effects and secondary ice production mechanisms

Arti Jadav



LUND
UNIVERSITY

DOCTORAL DISSERTATION

Doctoral dissertation for the degree of Doctor of Philosophy (PhD) at the Faculty of Science of Lund University, to be publicly defended on 12th of April 2024 at 13.00 in Världen Hall, Department of Physical Geography and Ecosystem Science, Sölvegatan 12, Lund, Sweden

Faculty opponent

Andrew Gettelman

Pacific Northwest National Laboratory, WA, USA

Organization Lund University Faculty of Science Department of Physical Geography and Ecosystem Science		Document name DOCTORAL DISSERTATION
		Date of issue 12 April 2024
Author Arti Jadav		Sponsoring organization
Title Improved Cloud Parameterization in Global Climate Model: Aerosol effects and secondary ice production mechanisms		
Abstract <p>The response of clouds to the changes in climate is uncertain, and the representation of the cloud-climate feedback is a key challenge in the global circulation models (GCM) for future climate projections. Factors contributing to this uncertainty include processes that involve particles of various sizes and phases, as well as the interactions between these particles and the surrounding atmosphere. The deep convective and stratiform cloud parameterizations in the Community Earth System Model (CESM) were improved and validated against the observations from the field campaign. These parameterizations explicitly resolve all known modes of heterogeneous cloud droplet activation, ice nucleation, secondary ice production (SIP) mechanisms, and growth processes, including collision/coagulation. The focus of the thesis is to improve the aerosols-cloud interaction and include the overlooked SIP mechanisms. A new detrainment scheme from a recent formulation based on high-resolution cloud modelling provides a better linkage between the convective and stratiform clouds. The mesoscale convective system (MCS) observed over Oklahoma, USA, during the Midlatitude Continental Convective Cloud Experiment (MC3E) was simulated with a single-column model, version 6 (SCAM6). The results are validated with ground measurements and in-situ aircraft observations. The analysis shows that the new microphysical parameterization provides a good representation of the ice initiation processes by including the empirically quantified primary ice processes and SIP mechanisms. Furthermore, the addition of SIP mechanisms has significantly improved the ice number concentrations in the mixed-phase regions of simulated MCS. Sensitivity experiments show that breakup in ice-ice collisions is predicted to be the most significant SIP mechanism in the simulations. Increasing the soluble aerosols resulted in reduced cloud particle sizes, inhibiting the growth of droplets, and thus enhancing the homogeneous cloud droplet freezing.</p>		
Key words Cloud, Primary ice, Secondary ice, Global climate model, cloud parameterization		
Classification system and/or index terms (if any)		
Supplementary bibliographical information		Language English
ISSN and key title		ISBN 978-91-89187-37-5 (print) 978-91-89187-38-2 (pdf)
Recipient's notes		Number of pages 87
		Price
		Security classification

I, the undersigned, being the copyright owner of the abstract of the above-mentioned dissertation, hereby grant to all reference sources the permission to publish and disseminate the abstract of the above-mentioned dissertation.

Signature _____

Date 12 April 2024

Improved Cloud Parameterization in Global
Climate Model:
Aerosol effects and secondary ice production
mechanisms

Arti Jadav



LUND
UNIVERSITY

Coverphoto by Arti Jadav

Funding information: Research grant to Vaughan Phillips (VTJP) from the Swedish Research Council for Sustainable Development (“FORMAS” Award 2018-01795), which supported the first author. This award concerns the effects on clouds and climate arising from the time-dependence of ice initiation.

Copyright pp 1-87 Arti Jadav

Paper 1 © by the Authors (Manuscript in revision)

Paper 2 © American Meteorological Society. Used with permission.

Paper 3 © CC-BY 4.0 License

Paper 4 © by the authors (Manuscript unpublished)

Faculty of Science

Department of Physical Geography and Ecosystem Science

ISBN: 978-91-89187-37-5

ISBN: 978-91-89187-38-2

Printed in Sweden by Media-Tryck, Lund University, Lund 2024



Media-Tryck is a Nordic Swan Ecolabel certified provider of printed material. Read more about our environmental work at www.mediatryck.lu.se

MADE IN SWEDEN 

યોમાસું

યોમાસું તો ખાસું ખૂબ,
દીસે દુનિયા ડૂબાડૂબ;
લોક ઉચ્ચારે રાગ મલાર,
ખેતર વાવે ખેતીકાર.
ચંપા ચમેલી જૂઈ જાય,
ફૂલ ગુલાબ ભલા ફુલાય;
છત્રી યોમાસે સુખ માટ,
ચાખડીઓ હીંડોળાખાટ.

કવીશ્વર દલપતરામ સી.આઈ.ઈ

Contents

List of publications	11
Author contributions	11
Paper I: An improved convection parameterization with detailed aerosol- cloud microphysics for a global model	12
Paper II: Effects from time dependence of ice nucleus activity for con- trasting cloud types	12
Paper III: The microphysics of the warm-rain and ice crystal processes of precipitation in simulated continental convective storms	12
Paper IV: A modified stratiform parameterisation for the Community Earth System Model	12
Acknowledgements	13
List of Figures	14

List of Symbols **21**

1 Introduction **23**

2 Background and Literature Review **25**

1 Atmospheric aerosols	25
1.1 Cloud condensation nuclei (CCN)	26
1.2 Ice nucleating particle (INP)	26
2 Basic Clouds types	26
2.1 Deep convective clouds	27
3 Cloud parameterisations	28
4 Cloud microphysical processes	29
4.1 Warm microphysical processes	29
4.2 Mixed- and ice-phase microphysics	30
Primary ice production mechanisms	31
Homogeneous freezing	31
Heterogeneous ice nucleation	31
Secondary ice production (SIP) mechanisms	32
Hallett-Mossop (HM) or Rime-splintering process	32
Fragmentation during ice-ice collisions	33

	Fragmentation during raindrop freezing	33
4.3	Precipitation formation	34
	Warm rain process	34
	Cold rain process	34
3	Aims and Scientific Hypotheses	37
1	Hypotheses	37
2	Objectives	38
4	Methods	39
1	Community Earth System Model and Single Column Atmospheric Model, version6	39
1.1	Convection Scheme	40
	Vertical velocity	40
	Evolution of cloud hydrometeors and aerosols	40
	Tagging tracers	41
	Aerosol treatment	41
	Cloud microphysics	41
	Initiation of cloud hydrometeors	42
	Cloud droplet activation	42
	Heterogeneous nucleation of cloud-ice	42
	Homogeneous freezing of cloud droplets	42
	Hallett Mossop process	42
	Fragmentation during ice-ice collisions	43
	Fragmentation during raindrop freezing	43
	Growth of cloud hydrometeors	43
	Condensational growth of cloud droplets	43
	Vapour growth of ice	43
	Autoconversion of cloud droplet to raindrop	43
	Autoconversion of cloud-ice to snow	43
	Autoconversion of snow to graupel	44
	Accretion, riming and aggregation processes	44
	Sedimentation of cloud hydrometeors	44
1.2	Stratiform scheme	45
2	Analysis of the role of time-dependent freezing of INPs	45
3	Aerosol-cloud (AC) model	46
4	Mid-latitude Continental Convective Clouds Experiment (MC3E) Cam- paign	46
4.1	11 May 2011 mesoscale convective system.	47
4.2	Airborne measurement	47
4.3	Ground based observation	48

5	Results	49
1	Implementation of new convective microphysics	49
1.1	SIP mechanisms	51
1.2	Soluble aerosol species in environment	53
1.3	Solid aerosol species in the environment	55
2	Analysis of the role of time-dependent freezing of INPs	56
2.1	Results from SCAM6	57
2.2	Results from the AC model	57
3	Analysis of the warm and cold rain processes	59
4	Implementation of the modified stratiform scheme in SCAM6	60
6	Discussions	63
7	Conclusion	67
1	References	69

List of publications

This thesis is based on the following publications, referred to by their Roman numerals:

- I **An improved convection parameterization with detailed aerosol-cloud microphysics for a global model**
Jadav, A., Waman D., Pant C.S., Patade S., Gautam M., Phillips V.T.J., Bansemer A., Barahona D., Storelvmo T.,
Manuscript conditionally accepted and in review at Journal for Atmospheric Sciences
- II **Effects from time dependence of ice nucleus activity for contrasting cloud types**
D., Waman, Patade S., A. Jadav, Deshmukh A., Gupta A.K., Phillips V.T.J., Bansemer A., Demott P.J.,
Journal for Atmospheric Sciences,80,2013–2039,<https://doi.org/10.1175/JAS-D-22-0187.1>
- III **The microphysics of the warm-rain and ice crystal processes of precipitation in simulated continental convective storms**
Gupta A.K., Deshmukh A., Waman D., Patade S., A. Jadav, Phillips V.T.J., Bansemer A., Martins J.A., Gonçalves F.L.T.,
Communications Earth & Environment,4,226(2023),<https://doi.org/10.1038/s43247-023-00884-5>
- IV **A modified stratiform parameterisation for the Community Earth System Model**
A. Jadav, Pant C.S., Waman D., Patade S., Phillips V.T.J.,
Manuscript unpublished

Author contributions

Co-authors are abbreviated as follows:

Arti Jadav (**AJ**), Vaughan TJ Phillips (VTJP),Ashok Kumar Gupta (AKG), Deepak Waman (DW), Chandra Shekar Pant (CSP)

Paper I: An improved convection parameterization with detailed aerosol-cloud microphysics for a global model

AJ and **VTJP** designed the study. **AJ** with the help of **VTJP** implemented the convective cloud parameterization and performed the simulations in the global model. **AJ** set up the input data to the model. **AJ** wrote the paper with contributions from all co-authors.

Paper II: Effects from time dependence of ice nucleus activity for contrasting cloud types

DW and **VTJP** conceptualized the study. The research was mostly performed by **DW**. **AJ** provided the input data for the **MC3E** simulations performed by **DW**. **AJ** was involved with the model validation and in the preparation of the manuscript.

Paper III: The microphysics of the warm-rain and ice crystal processes of precipitation in simulated continental convective storms

AKG and **VTJP** conceived the study. The research was mostly performed by **AKG**. **AJ** provided the input data to set up the **MC3E** case in the model and helped in reviewing the manuscript.

Paper IV: A modified stratiform parameterisation for the Community Earth System Model

VTJP designed the study. **CSP** started the implementation of the stratiform microphysics parametrization in the global model. **AJ** with the help of **VTJP** carried on the work started by **CSP** and finished the implementation of the new stratiform cloud parameterization and performed the simulations in the global model. **AJ** wrote the paper with contributions from all co-authors.

Acknowledgements

During my PhD, I have been fortunate to receive support, guidance, and inspiration from many individuals who have contributed to the successful completion of this work. First of all, I'd like to thank my supervisor, Dr. Vaughan T.J. Phillips, for his ideas, support, knowledge and guidance throughout the entire duration of my PhD. I really appreciate your support in combining my work into a coherent research project.

Petter Pilsejö, thank you for your invaluable support, kindness and encouragement. You motivated me continuously to move forward, and now I can say I reached the light at the end of the tunnel. You encouraged me to stay positive and helped me persevere and overcome challenges along the way.

I would like to acknowledge and thank the co-authors for their collaboration and contributions to this project, Trude Storelmov, Donifan Barahona, Aaron Bansemer, Deepak Waman, and Sachin Patade. I want to thank Chandra Shekhar Pant for their insightful discussion and great feedback on my research work.

Many thanks to the colleagues and friends at INES: Adrian, Alexandra, Ali, Andreas, Carlos, Deepak, Freddy, Hanna, Hao, Jalisha, Jean-Nicolas, Joel, John, Johan, Karin, Karolina, Kimberely, Lina, Mahendra, Micael, Mitro, Nuwanthi, Olive, Patrick, Pengxiang, Pheaktra, Renkui, Ross, Sofia, Tetiana, Tristan, Xueying and Yanzi. A special thanks to Antje, Deborah, and Shubham for all the dinner parties, fikas, hikes, office chats, and always being there for me. I cherish these memories. Asmita, I very much enjoyed our hour long phone calls and trips through Sweden.

I am grateful to my wonderful parents for their constant love and support. I appreciate the unconditional care, video calls, and unwavering belief in me. Many thanks to my siblings and brother-in-law for their affection and delicious meals. A special shoutout to Daniel, my partner, for his love, patience, and consistent support. You have a way of lifting my spirits and bringing a smile to my face on difficult days. And last but not least, heartfelt thanks to my furry companions Lex, Becky, and Cupcake for being cute little cuddly monsters.

I am deeply grateful to all these individuals for their invaluable contributions, support, and encouragement throughout my PhD journey.

List of Figures

2.1	Schematic representation of homogeneous and four mechanisms of heterogeneous ice nucleation (from Khain and Pinsky (2018a) after Vali (1999)). processes	31
4.1	A Skew-T Log-P diagram showing the atmospheric profiles of temperature (solid black line), dew point temperature (solid blue line) for the initial simulation time of 00 UTC on 10 May 2011	47
5.1	Predicted (a) CDNC compared with CDP probe data, (b) LWC compared with CDP, KING and Nevzorov probe data, (c) vertical velocity, (d) total number concentration of ice particles with sizes greater than 0.2mm compared with 2DC, CIP, HVPS-3 probe data and COMB data, (e) total ice number concentrations of ice particles with size greater than 1 mm compared HVPS-3 probe data (f) total ice particle mass mixing ratio from the SZ11 (solid red line with square) and ACC (solid black line with pentagram) simulations. The cloud microphysical properties are conditionally averaged over cloudy convective updrafts ($w_{up} > 3 \text{ m s}^{-1}$). Predicted (g) precipitation rate mm/hr and (h) accumulated surface precipitation compared with observations (Xie et al., 2014). Predicted (i) stratiform and convective cumulative precipitation from the SZ11 and ACC_24 simulations.	51

- 5.2 (a) Comparison of the predicted total number of cloud-ice from the SIP mechanism in the simulation compared with predicted total cloud-ice. (b) The contributions from cloud-ice (dotted line with diamond), graupel/hail (dotted line with triangle) and snow (dotted line with square) are plotted, as well as total ice (solid line with pentagram). Bar plot for the (c) budgets of the number of cloud-ice particles and (d) budget of the mass mixing ratio of cloud-ice particles initiated from heterogeneous ice nucleation ('Het. nuc.'), homogeneous freezing ('Hom. frz.'), fragmentation during ice-ice collisions ('Breakup'), fragmentation during raindrop freezing ('Rfz') and HM process. Bar plot of the (d) budgets of the number and (e) budget of the mass mixing ratio of cloud-ice, snow and graupel particles initiated in the cloud for the ACC_24 simulation. The cloud microphysical properties are conditionally averaged over cloudy convective updrafts ($w_{up} > 3 \text{ m s}^{-1}$). 53
- 5.3 Vertical profiles of predicted (a) mean cloud droplet diameter, (b) LWC and (c) CDNC plotted with secondary droplets, (d) surface precipitation rate (mm hr^{-1}), (e) cumulative surface precipitation (mm) and (f) total ice particle number concentration with tagging tracers for cloud-ice initiated from primary ice processes ('prim.') (dotted line), HM process (dash-dotted line), and (i) total ice particle number concentration with tagging tracers for cloud-ice initiated from breakup in ice-ice collisions ('Brk') (dotted line), raindrop freezing fragmentation process ('Rfz') (dashdotted line) from the high-CCN (solid red line with squares), low-CCN (solid blue line with diamond) and ACC_24 (solid black line with pentagram) simulations. The cloud microphysical properties are conditionally averaged over cloudy convective updrafts ($w_{up} > 3 \text{ m s}^{-1}$). Bar plot for the (g) budgets of the number of cloud-ice particles initiated from heterogeneous ice nucleation ('Het. nuc.'), homogeneous freezing ('Hom. frz.'), breakup in ice-ice collisions ('Breakup'), raindrop freezing fragmentation ('Rfz') and HM process and (h) budgets of the number of cloud-ice, snow and graupel particles initiated in the cloud for the ACC_24 (black coloured bars), high-CCN (red coloured bars) and low-CCN (blue coloured bars) simulations. 55

5.4 (a) Predicted mean cloud droplet diameter, (b) predicted LWC and (c) predicted CDNC plotted with secondary droplets, (d) surface precipitation rate (mm hr^{-1}), (e) cumulative surface precipitation (mm) and (f) total ice particle number concentration with tagging tracers from cloud-ice from primary ice processes ('prim.') (dotted line), HM process (dash-dotted line), and (i) total ice particle number concentration with tagging tracers from breakup in ice-ice collisions ('Brk') (dotted line), raindrop freezing fragmentation process ('Rfz') (dash-dotted line) from the high-INP (solid red line with squares), low-INP (solid blue line with diamond) and ACC_24 (solid black line with pentagram) simulations. The cloud microphysical properties are conditionally averaged over cloudy convective updrafts ($w_{up} > 3 \text{ m s}^{-1}$). Bar plot for the (g) budgets of the number of cloud-ice particles initiated from heterogeneous ice nucleation ('Het. nuc.'), homogeneous freezing ('Hom. frz.'), breakup in ice-ice collisions ('Breakup'), raindrop freezing fragmentation ('Rfz') and HM process and (h) budgets of the number of cloud-ice, snow and graupel particles initiated in the cloud for the ACC_24 (black coloured bars), high-INP (red coloured bars) and low-INP (blue coloured bars) simulations. 56

5.5 Predicted (a) mean cloud droplet diameter, (b) LWC, (c) CDNC, (d) total number concentration of ice particles, (e) tagging tracer representing the cloud-ice generated by Heterogeneous ice nucleation from the Time dependence (solid red line with square) and ACC_24 (solid black line with pentagram) simulations. The cloud microphysical properties conditionally averaged over cloudy convective updrafts ($w_{up} > 3 \text{ m s}^{-1}$). Predicted (f) cumulative surface precipitation from the Time dependence (solid red line with square) and ACC_24 (solid black line with pentagram) simulations are plotted. 57

- 5.6 (left) The predicted number concentrations of active INPs conditionally averaged over stratiform regions ($|\mathbf{w}| < 1$ m/s) from mineral dust (solid line with open circles), soot (solid line with asterisks), and PBAP (solid line with squares), and concentrations of heterogeneously nucleated ice (PRIM-ICE, forward-pointing triangles) for the (a) MC3E, (c) ACAPEX, and (e) APPRAISE cases. The same information is shown with dotted lines for the “no time-dependent INP” run. (right) The concentrations of total nonhomogeneous ice (total cloud ice and snow minus total homogeneous ice; solid line with squares) and various tracer terms defining SIP processes such as fragmentation during sublimation (FSB; solid line with asterisks), ice–ice collisions (FIIC; solid line with pentagrams) and raindrop freezing (FRF; solid line with upward-pointing triangles), and the HM process (HM; solid line with open circles) for the (b) MC3E, (d) ACAPEX, and (f) APPRAISE case, respectively. The same information is shown with the dotted lines for the “no time-dependent INP” run. To compare the number concentrations of heterogeneously nucleated ice and total nonhomogeneous ice, heterogeneously nucleated ice (PRIM-ICE; forward-pointing triangles) is also shown in the right column. The figure is adapted from Waman et al. (2023). 58
- 5.7 Temperature-resolved conditionally averaged over cloudy regions of: a mass mixing ratio (MMR) and b number mixing ratio (NMR) of graupel with corresponding warm (red line) and cold (blue line) components; c mass and d number mixing ratios of rain plotted similarly; e ice (orange) and snow (brown) mass mixing ratio; f ice (light blue) and snow (magenta) number mixing ratio; and g cloud water number mixing ratio (purple) for the MC3E case (slightly warm-based convective clouds at 17°C) control simulation using AC during 0000–2300 UTC on 11 May 2011. Also shown is the MC3E case control simulation of the accumulated precipitation (mm) for h the entire domain with all clouds and corresponding components from i convective and j stratiform cloudy (and adjacent clear sky) regions for 72h (10–13 May 2011). The yellow and gray shading boxes in (a–g) are similar to those in Fig. 2, with differences in (b) and (e). b The darkest gray shaded box represents cold rain mass mixing ratio, while medium gray is for warm. e The darkest yellow displays the peak value of ice mass mixing ratio, while medium yellow is for snow. The figure is adapted from Gupta et al. (2023). 60

5.8	Predicted (a) precipitation rate (mm/hr), (b) cumulative surface precipitation, (c) LWC (g m^{-3}) with CDP, KING and Nevzorov probes, (d) CDNC (cm^{-3}) compared with observations from the CDP probe, from the MG08 (dashdotted black line with square) and LLS24 (solid black line) simulations. Error bars shown are standard errors of observation samples. The cloud microphysical properties are conditionally averaged over the entire simulation period.	61
5.9	Predicted (a) total concentration of ice particles with sizes $> 0.2\text{mm}$ compared with observations from the 2DC, CIP, HVPS-3 probe and COMB, (b) total ice number concentrations of all ice particles with size $> 1 \text{ mm}$ compared with aircraft observations from the HVPS-3 probe and (c) total IWC from the MG08 (dashdotted black line with square) and LLS24 (solid black line) simulations. Error bars shown are standard errors of observation samples.	62

List of Tables

4.1	The microphysical conversion tendencies for mass mixing ratio ($\text{kg}^{-1}\text{kg}^{-1}\text{s}^{-1}$). The first symbols within the parentheses before the semicolon represent the final species in each interaction. The symbols after the semicolon represent the interacting species. The table is a modified version of Phillips et al. (2007, Table 1.).	44
4.2	Meteorological instruments carried on Citation <i>II</i> aircraft	48

Acronyms

- 2DC** 2D Cloud imaging probe. 14, 48, 51
- AC** Aerosol-cloud. 9, 10, 38, 46, 56, 57, 59, 63, 65, 68
- ACC** new aerosol-cloud convection. 40
- AR6** Sixth Assessment Report. 24
- CAM6** Community Atmosphere Model, version 6. 39, 40, 45
- CCN** Cloud condensation nuclei. 8, 26, 29, 33
- CDNC** cloud droplet number concentration. 14–16, 30, 42, 49, 51, 54–57, 61
- CDP** Cloud droplet probe. 14, 48, 51
- CESM** Community Earth System Model. 9, 39
- CF** Central Facility. 46, 47
- CFDC** Continuous Flow Diffusion Chamber. 42
- CIP** Cloud Imaging Probe. 14, 48, 51
- CKE** collision kinetic energy. 43
- EP** Empirical parameterization. 42, 45
- GCMs** general circulation models. 24
- GPM** Global precipitation measurement. 46
- HM** Hallett-Mossop. 8, 32, 33

HVPS-3 High-volume precipitation spectrometer, version 3. 14, 48, 51

ICNC ice crystal number concentration. 33

INP Ice nucleating particle. 8, 26, 31, 32, 37, 38, 42

INSPECT Ice Nuclei Spectroscopy. 42

IPCC Intergovernmental Panel on Climate Change. 24

LCL Lifting condensation level. 47

LWC liquid water content. 14–16, 49, 51, 54–57, 61, 63, 64

MC3E Mid-latitude Continental Convective Clouds Experiment. 9, 46

MCS mesoscale convective system. 47

NASA National Aeronautics and Space Administration. 46, 47

PBAPs Primary Biological Aerosol Particles. 46

PBL planetary boundary layer. 64

SBM spectral bin microphysics. 28

SCAM6 Single Column Atmospheric Model, version 6. 9, 10, 38, 39, 56, 57, 60, 63, 65

SCE stochastic collection equation. 30

SCM Single Column Model. 39

SIP Secondary ice production. 8, 32, 38

TOA top of atmosphere. 23

UND University of North Dakota. 47

WBF Wegener-Bergeron-Findeisen. 35, 45

WRF Weather Research and Forecasting. 46

List of Symbols

Symbol	Description	Units
X	solid aerosol species (X = mineral dust, black carbon, insoluble biological aerosols, and primary organic matter)	-
A_X	Fitting constant for the temperature shift in the solid aerosols	-
e	vapour pressure	Pa
e_s	saturation vapour pressure	Pa
E_u	Entrainment rate	s^{-1}
Q	Passive tracer to calculate the age of the parcel since entering the subzero part of the cloud	kg^{-1}
Q_0	Initial passive tracer value when the parcel is outside the glaciated part of the cloud	$1 kg^{-1}$
q_v	Vapour mass mixing ratio	$kg kg^{-1}$
q_c	Cloud droplet mass mixing ratio	$kg kg^{-1}$
q_i	Cloud-ice mass mixing ratio	$kg kg^{-1}$
q_s	Snow mass mixing ratio	$kg kg^{-1}$
q_r	Rain mass mixing ratio	$kg kg^{-1}$
q_g	Graupel/hail mass mixing ratio	$kg kg^{-1}$
\tilde{t}	time since the start of the isothermal phase of the laboratory experiment Jakobsson et al. (2022)	s
X_{cld}	Conserved variables such as mass and number mixing ratio of cloud liquid, cloud-ice, rain, snow, graupel/hail and actual number mixing ratio for each size bin of the aerosols in any given chemical species (e.g., sulphate, dust, sea salt)	when X_{cld} represents mass mixing ratio, then the unit is $kg kg^{-1}$ and when X represents number mixing ratio, the unit is kg^{-1}
$S_{X_{cld}}$	source/sink term corresponding to subscript X_{cld}	units of X_{cld}
X_{env}	Environmental value of cloud hydrometeor corresponding to X_{cld}	units of X_{cld}
β	Fitting constant for temperature shift in time-dependent freezing of INP	-
ΔT_X	Temperature shift due to time-dependent INP freezing	K
Δt	Time step for the parcel ascent	0.025 s

Chapter 1

Introduction

The Earth's climate system is driven by the radiative energy balance at the top of atmosphere (TOA) between the incoming shortwave radiation and outgoing longwave radiation. The complex processes within the atmosphere, land, ocean, and biosphere work over time-space scales to modulate the distribution of absorbed, scattered and emitted radiation.

Clouds play a crucial role in the Earth's climate system by influencing Earth's energy budget and hydrological cycle. Clouds reflect the incoming shortwave radiation (cooling effect) and absorb or re-emit the outgoing longwave radiation (greenhouse effect). The globally averaged radiative energy resulting from these two effects determines the net impact on the Earth's energy budget. At present climate, clouds provide a cooling effect by reducing the net downward radiation at TOA by 20 Wm^{-2} (Harrison et al., 1990; Forster et al., 2021).

In the present climate system, almost 70% of the globe is covered by clouds (Stubenrauch et al., 2013; Eytan et al., 2020). Modern aerosol emissions indirectly impact cloud albedo by increasing the droplet number concentration and decreasing the average droplet size (Twomey, 1974; Albrecht, 1989). This enhances cloud albedo, offsetting an uncertain fraction, perhaps, approximately half of the global warming attributed to greenhouse gas emissions since pre-industrial times (Lohmann, 2006). A warm cloud or, liquid-only cloud, or low-level cloud has a high albedo, which means such clouds are effective at reflecting incoming sunlight back to space (Hartmann et al., 1992). As a result, low-level clouds can cool the Earth's surface. In contrast, high-level clouds can warm the surface as they have a lower albedo than low-level clouds and enhance the greenhouse effect by trapping longwave radiation (McFarquhar et al., 2000; Hang et al., 2019).

Since the pre-industrial period, the Earth's surface and atmosphere have warmed, altering the macrophysical (e.g. altitude, cloud fraction) and microphysical properties (phase, cloud ice number concentration, particle size) of clouds. Changes in the cloud properties and extend induces climate change by creating a "*cloud feedback*". The cloud feedback can either amplify or offset future warming. According to the Sixth Assessment Report (AR6) of the Intergovernmental Panel on Climate Change (IPCC) (Forster et al., 2021), the equilibrium climate sensitivity estimates from general circulation models (GCMs) is likely to lie in the range 2° to 5°C. The most significant contribution to overall uncertainty is from the cloud feedback. For cold clouds (mixed-phase or ice-only) the partitioning of supercooled cloud-liquid between ice and liquid phases affects the climate sensitivity (Tan et al., 2018; Sherwood et al., 2020; Zelinka et al., 2023). Therefore, understanding the factors that govern clouds and how they will behave in a changing climate is essential for accurately predicting future climate scenarios.

Chapter 2

Background and Literature Review

1 Atmospheric aerosols

Atmospheric aerosols are solid or liquid particles suspended in air. Typically, their concentration is 1 to 10^6 per cm^3 of air, with high concentrations over continents (Takemura, 2012; Pringle et al., 2010). These particles exhibit a wide size range, spanning from nanometers to tens of micrometres.

Aerosols significantly influence the climate system through both direct and indirect radiative effects. The "direct effect" involves the scattering and absorption of shortwave and longwave radiation contingent on aerosol properties (Forster et al., 2021). Indirect effects pertain to how aerosols modulate cloud formation and properties, subsequently impacting Earth's atmospheric radiation balance (Twomey, 1977; Albrecht, 1989). Human activities, including greenhouse gas emissions and aerosol emissions, substantially contribute to alterations in the climate system. Understanding the augmented aerosol emissions resulting from increased human activity is pivotal for comprehending aerosols' role in the climate system.

Aerosols emanate from diverse sources, including natural sources such as volcanic eruptions, seaspray, and anthropogenic sources like vehicular traffic. They enter the atmosphere as either primary particulate or secondary particulate matter.

Aerosols can be categorised into primary particles, comprising dust from deserts or arid regions, pollen, and soot from incomplete fossil fuel combustion, and secondary particles formed in the atmosphere through gas-to-particle conversion processes. These processes encompass nucleation, condensation, and coagulation from vapour, known as aerosol precursors, which include sulfur dioxide, nitrogen oxides, volatile organic

compounds, and ammonia.

Various processes contribute to aerosol removal from the atmosphere, including gravitational settling, dry deposition, and wet deposition, the latter of which is further classified into in-cloud scavenging and below-cloud scavenging. In-cloud scavenging involves aerosols being taken up into cloud droplets, while below-cloud scavenging pertains to their removal from the atmosphere through precipitation events.

1.1 Cloud condensation nuclei (CCN)

Hygroscopic aerosols are expected to nucleate cloud droplets (Petters and Kreidenweis, 2007). They mostly comprise of sulfates, soluble organic matter, ammonium, and sea salt (Pruppacher and Klett, 2010). The majority of CCN consist of aerosols with sizes $> 0.1\mu\text{m}$ because aerosols with sizes $< 0.1\mu\text{m}$ require higher supersaturation to nucleate (Köhler, 1936).

1.2 Ice nucleating particle (INP)

INP particle can nucleate ice in four different modes, *condensation*, *deposition*, *immersion* and *contact* nucleation (Meyers et al., 1992; Phillips et al., 2008). The chemical composition, temperature and size determine the effectiveness of an INP to nucleate ice.

2 Basic Clouds types

"Clouds are the sleeping giant of the climate system: David Archer"

Clouds form when moist air ascends and cools below its dew point, causing water vapour to condense into droplets or ice crystals. The ascent of moist air occurs through various mechanisms, such as orographic lifting, frontal lifting, convection, or convergence of air masses Rogers and Yau (1996).

Since early scientific research (Lamarck, 1802; Howard, 1803) clouds have been primarily classified into three categories, namely, *stratiform*, *convective* and *cirrus* clouds based on their visual appearance (Lohmann et al., 2016).

Stratiform clouds are characterised by their layered or sheet-like structure, often covering large horizontal distances (Houze, 2014). They have a weak vertical velocity,

leading to extended durations and continuous precipitation. Stratocumulus develops as a result of the convective processes, often capped by a stable layer of air aloft, which acts as a lid, preventing further vertical development of the clouds, making them similar to *stratus* clouds (Wood, 2012, 2015; Houze, 2014).

Cirrus clouds are wispy, high-altitude clouds that are composed of ice crystals. They are commonly found at high levels in the atmosphere. The outflow of the anvils from the deep convective clouds can lead to the formation of cirrus clouds, which then spread laterally in the troposphere (Mace et al., 2006; Sassen et al., 2008; Houze, 2014).

Convective clouds, in contrast to the widespread nature of cirrus and stratus clouds, are more localised and have a vertical extent similar to their horizontal extent. They are characterised by strong vertical velocities and rapid evolution, leading to shorter lifetimes compared to stratiform clouds (Houze, 2014). Various categories of convective clouds exist based on the evolution of their vertical extent. Shallow cumulus clouds, driven entirely by warm-phase processes, typically have lifetimes of a few tens of minutes and are commonly seen in temperate latitudes as "fair-weather clouds." Cumulus congestus exhibits stronger vertical motions and the development of individual towers reaching the lower troposphere but still mainly consists of liquid water droplets as the buoyant air rises and comes to the layers of the atmosphere with temperatures below 0°C; further latent heat is released due to the freezing of liquid water. This transforms cumulus congestus clouds into fully developed deep convective cumulonimbus clouds. These clouds are characterised by their towering vertical extent and are associated with strong updrafts and downdrafts, intense precipitation, thunderstorms, and sometimes severe weather conditions.

As the focus is on implementing a new parameterisation for deep convective clouds in this thesis, salient aspects of their structure and evolution are described in detail in the following sect. 2.1, before introducing the most important aspects of the detailed microphysical processes in sect. 4

2.1 Deep convective clouds

Deep convective clouds vertically transport heat, humidity, and momentum in the atmosphere, thus affecting the large-scale atmosphere. Deep convection plays a crucial role in tropical climate systems, including the formation of Hadley cells (Bony et al., 2015) and tropical cyclones (Tory et al., 2006). They affect the mid-latitude weather patterns, including the formation of extratropical cyclones and the movement of weather systems (Smull, 1995; Doswell, 2001).

The updrafts in intense convective clouds can reach vertical velocities of 10 to 20 m/s

(Heymsfield and Hjelmfelt, 1984; Heymsfield et al., 2005). Depending on the geographical location, these clouds can go up to 10 to 17 km altitude above mean sea level and rarely extend 1.5 km above the tropopause (Gettelman et al., 2002). At the cloud top, the air mass spreads out in the shape of a striated anvil composed of only ice hydrometers, that can cover large areas, while the lower portion resembles a mountain of individual towers.

Convective parameterisations describe the collective impact of all convective clouds within a grid box on the large-scale variables because of their localised nature (Arakawa, 2004).

3 Cloud parameterisations

The cloud hydrometeors are categorised into cloud liquid, rain, cloud ice, snow and graupel/hail. The two approaches to treating cloud parameterisation are *bulk microphysics scheme* and *bin microphysics scheme* (Khain et al., 2015).

The first approach is bulk parameterisation, which represents particle size distributions (PSDs) of each hydrometer, commonly by a gamma or exponential distribution. Single-moment bulk schemes consider only mass mixing ratio of each hydrometer species (Kessler, 1969; Lin et al., 1983; Tao and Simpson, 1993; Walko et al., 1995; Kong and Yau, 1997). Double-moment bulk schemes include prognostic treatment of a mass mixing ratio and number mixing ratio (Ziegler, 1985; Wang and Chang, 1993; Ferrier, 1994; Meyers et al., 1997; Seifert and Beheng, 2001; Morrison et al., 2005; Morrison and Gettelman, 2008). Double-moment schemes generally perform better than single-moment schemes because of the inclusion of the effect of aerosols on the number concentration and sizes of hydrometeors (Igel et al., 2015; Khain et al., 2015). Three-moment bulk schemes include mass mixing ratio, number mixing ratio, and radar reflectivity (Milbrandt and Yau, 2005a,b).

The second approach is spectral bin microphysics (SBM), also known as size-resolving microphysics. SBM resolves particle size distributions on a mass grid containing many discrete size bins, ranging from tens to hundreds. SBM provides a more accurate representation of various physical processes, including different collection processes. The main advantage of SBM is that it treats the liquid phase, eliminating the need for separating cloud droplets and raindrops as required in bulk schemes. Due to complex shapes and properties, ice-phase hydrometeors are generally classified into individual categories, similar to bulk schemes. The computation of numerous microphysical interactions results in an increased number of advected prognostic variables, about 200-300, whereas the bulk schemes have 6-18 variables. The detailed description makes SBM

computationally expensive compared to bulk schemes.

A third approach, involves the emulating bin schemes which represents cloud microphysical processes by combining SBM and bulk approaches (Cotton et al., 2003; Saleeby and Cotton, 2004; Kudzotsa et al., 2016). This scheme involves the size distribution of hydrometeors being represented with temporary grid of discrete size bins for specific microphysical processes while reducing the size distribution to double- or three-moment for advection and diffusion.

4 Cloud microphysical processes

Cloud microphysical processes involve the interactions between the cloud hydrometeors, aerosols, and phase change within cloud systems. These processes occur at micro to centimetre scales within the cloud. Cloud microphysics is parameterised to represent the overall effect on cloud dynamics and precipitation processes in numerical weather models, ranging from high-resolution large eddy simulations with grid box sizes of tens of meters to global models with grid box sizes of hundreds of kilometres (Khain et al., 2015; Rio et al., 2019). These processes exert feedback to the dynamic development of clouds by latent heat release that increases the buoyancy and are influenced by the dynamics and thermodynamics of the environment (Rogers and Yau, 1989; Khain et al., 2015).

4.1 Warm microphysical processes

Warm phase processes determine the boundary and initial conditions relating to hydrometeors, moisture, and heat transfers to the mixed and cold phases of clouds.

Aerosols in the atmosphere are crucial for the formation of cloud droplets. As air rises and cools, water vapour condenses on aerosols to form cloud droplets called heterogeneous nucleation. Water soluble aerosols act as CCN, and their activation depends on their chemical composition and size. Köhler's theory describes the CCN activation. The theory combines the Raoult and Kelvin effect.

The Raoult effect refers to the impact of solute molecules on the saturation vapour pressure of a solution droplet. According to the Raoult effect, the presence of solute molecules in the liquid reduces the saturation vapour pressure of the solution compared to pure water. This reduction in saturation vapour pressure means that the droplet must be at a lower vapour pressure than its surrounding environment to maintain equilibrium. As a result, the droplet requires a higher relative humidity to achieve saturation and

continue growing.

The Kelvin effect states that the saturation vapour pressure of a droplet is influenced by its curvature. For a tiny droplet, the saturation vapour pressure is higher on the curved surface than the surrounding air. As the droplet grows, its curvature decreases, and the difference in saturation vapour pressure between the droplet and the surrounding air diminishes. This implies that larger droplets require lower relative humidity to maintain saturation than smaller droplets.

The Köhler theory is given as,

$$\frac{e}{e_s} = 1 + \frac{a}{r} - \frac{b}{r^3} \quad (2.1)$$

where $\frac{e}{e_s}$ is supersaturation ratio, $\frac{a}{r}$ is Kelvin effect and $\frac{b}{r^3}$ is Raoult effect (Lamb and Verlinde, 2011; Houze, 2014)). Hygroscopic or solute aerosol particles with large sizes ($> 0.2\mu\text{m}$) would activate to become cloud droplets.

Droplets grow by water vapour diffusion and condensation reaching up to about 0.1mm in diameter (Rogers and Yau, 1989).

Raindrops grow by *accretion*, which involves a collision between cloud droplets and raindrops. Accretion is more efficient than autoconversion and significantly contributes to overall rain production (Kogan, 2013; Hill et al., 2015).

The *autoconversion* parameterisation describes the raindrop formation from the collision between cloud droplets. In bin schemes and emulating bin schemes, autoconversion is expressed through numerical solutions of the stochastic collection equation (SCE) for various bin sizes (Benmoshe and Khain, 2014; Khain et al., 2015). In bulk schemes, the parameters for the autoconversion are derived from regression analysis of the solution to SCE using results from numerous detailed bin-microphysics simulations (Seifert et al., 2010; Khain et al., 2015). Morrison and Gettelman (2008); Song and Zhang (2011); Kudzotsa et al. (2016) implements a semiempirical formulation based on results from LES simulations with a bin-microphysics from Khairoutdinov and Kogan (2000). The parameterisation represents an increased transfer from droplets to rain with increased cloud water content but a decrease with increased cloud droplet number concentration (CDNC). These relationships represent the increase in autoconversion rate with increased cloud water content and a reduction with increased CDNC.

4.2 Mixed- and ice-phase microphysics

The mixed phase refers to cloud layers containing liquid particles and ice crystals. Cold-phase or ice-phase refers to cloud layers consisting of only ice crystals. Ice crys-

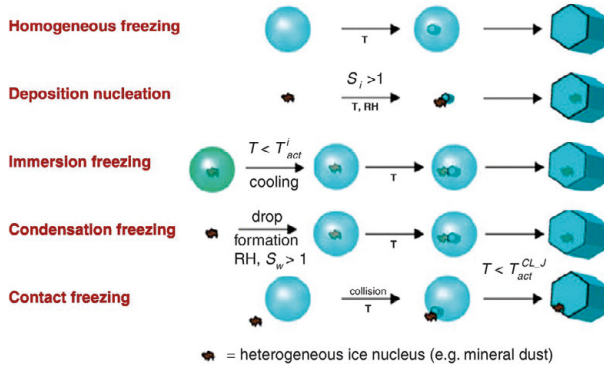


Figure 2.1: Schematic representation of homogeneous and four mechanisms of heterogeneous ice nucleation (from Khain and Pinsky (2018a) after Vali (1999)). processes

tals. Cold microphysical processes deal with microphysical processes involving ice crystals. Representation of cold microphysics in numerical models is challenging because it consists of a transition between three phases (gas, liquid, and solid), and ice crystals exhibit a wide variety in shape and density (Pruppacher and Klett, 2010; Khain and Pinsky, 2018b). In most microphysics schemes, ice crystals are separated into different categories, such as cloud-ice, snow, graupel/hail (Kudzotsa et al., 2016; Waman et al., 2023).

Liquid hydrometeors (cloud droplets and rain) can exist as supercooled drops below freezing. They can reach up to levels with temperatures as low as -35°C and remain unfrozen (Anderson et al., 1980; Hirst et al., 2001). Ice formation occurs from primary and secondary ice processes.

Primary ice production mechanisms

The primary ice production mechanisms involves *homogeneous* and *heterogeneous* freezing of liquid hydrometeors (Rogers and Yau, 1989; Khain and Pinsky, 2018b).

Homogeneous freezing Homogeneous freezing refers to the spontaneous freezing of cloud droplets in the absence of nucleating particles at very low temperatures ($\sim -35^{\circ}\text{C}$). Typical temperatures used in microphysics schemes are -40°C Morrison and Gettelman (2008); Song and Zhang (2011) and -36°C by Phillips et al. (2007).

Heterogeneous ice nucleation Supercooled droplets freeze in the presence of INPs to form ice crystal (Vali, 1996; Vali et al., 2015). The first ice crystal in the cloud

is formed from this process. The are four mechanisms of heterogeneous freezing are (Rogers and Yau, 1989; Khain and Pinsky, 2018a; Kanji et al., 2017):

- Water vapour directly deposits on the INPs to form ice crystals, referred to as *deposition freezing*.
- Water vapour condenses on the surface of water covered INPs and freezes to form ice crystals, referred to as *condensation freezing*.
- Supercooled droplets come into contact with active INPs and freeze to form ice crystals, referred to as *contact freezing*.
- INP is immersed in a droplet at warm temperatures ($> 0^{\circ}\text{C}$). At cold temperatures ($< 0^{\circ}\text{C}$), freezing is initiated by the immersed INPs. This mechanism is referred to as *immersion freezing*

Nucleation rate is an important parameter for parameterising homogeneous freezing. In SBM, the nucleation rate is used to derive the number of ice crystals produced by droplets in each size bin (DeMott et al., 1994). In bulk parameterisation, total number of ice crystals is calculated from the homogeneous freezing rate (Liu and Penner, 2005; Phillips et al., 2007). The freezing rates for the bulk parameterisation were derived from fitting the results of a spectral microphysics parcel model, run over a wide range of aerosol concentrations and vertical velocities in upper troposphere.

Secondary ice production (SIP) mechanisms

SIP mechanisms enhance ice crystal concentration from preexisting ice crystal without the action of INPs (Yang et al., 2016; Field et al., 2016; Korolev and Leisner, 2020) under suitable conditions. Observations show that ice number concentrations are orders of magnitudes higher than the INP concentrations Gardiner and Hallett (1985); DeMott et al. (2003); McFarquhar et al. (2006); Ladino et al. (2017). The proposed SIP mechanism are (Field et al., 2016) are as follows:

Hallett-Mossop (HM) or Rime-splintering process Hallett and Mossop (1974) observed small ice splinters were produced during the riming of supercooled drop with size $> 24\mu\text{m}$ in the temperature range -3° to -8°C . For levels above -3°C , supercooled drops do not form ice shells (Dong and Hallett, 1989). Additionally, for levels below -8°C , hard ice shell cannot be fractured from internal pressure (Griggs and Choulaton, 1983).

Field experiments and aircraft observations (Harris-Hobbs and Cooper, 1987; Blyth and Latham, 1993; Rangno and Hobbs, 2001; Crosier et al., 2011; Lasher-Trapp et al., 2016) observed graupel/hail or rimed ice in the HM region.

The activity of HM process varies with cloud types and depends on temperature, presence of rimed ice and size of supercooled drops. For a cloud with high CCN concentration, there would be numerous small drops, which would result in a reduced activity of the HM process.

SBM calculates the number of collisions between graupel/hail and drops at each time step (Qu et al., 2020). Cotton et al. (1986) provided a bulk parameterisation for the number of ice splinters produced per gram of the accreted liquid drop, according to Hallett and Mossop (1974). Various microphysics scheme (Song and Zhang, 2011; Kudzotsa et al., 2016) utilities the formulation by Cotton et al. (1986).

Fragmentation during ice-ice collisions Fragmentation during ice-ice collisions is another important microphysical process in ice-phase clouds. Ice crystals collide, which may result in mechanical breakup, leading to the production of secondary ice (Langmuir, 1948). Several field and laboratory studies later confirmed this theory (Hobbs and Farber, 1972; Takahashi et al., 1995; Vardiman, 1978). A study by Schwarzenboeck et al. (2009) pointed out 20% - 80% of the ice crystals are naturally fragmented, possibly due to collisions of ice crystals. Their simulations for crystal break-up showed a good agreement with the experimental data.

Hobbs and Farber (1972); Yano and Phillips (2011); Yano et al. (2016); Phillips et al. (2017a,b) conducted theoretical studies and demonstrated multiplication in ice number from this process. Sullivan et al. (2017) demonstrated from their parcel model simulations that rime splintering and breakup in graupel-graupel collisions enhance ICNC up to 4 orders of magnitude. Sullivan et al. (2018b) showed that ice-ice collisional breakup is the most significant SIP mechanism. Sotiropoulou et al. (2020) observed that the high ice crystal number concentration (ICNC) cannot be explained by primary ice processes. They conclude including rime splintering and collisional break-up provides better agreement with observations in the summer Arctic stratocumulus cloud. Sotiropoulou et al. (2021) found that model with ice-ice collisional breakup improves the prediction of ICNC and suggested this mechanism can generate significant fragments from 0.1 L^{-1} of primary ice.

Fragmentation during raindrop freezing Another SIP mechanism is the fragmentation of a freezing drizzle or raindrop. It involves the process by which ice particles are formed as a result of the freezing of supercooled liquid droplets. When a supercooled

droplet freezes, water may be trapped inside the ice shell around the droplet. As the water turns into ice, it expands which generates mechanical pressures inside the droplet. If these pressures are high enough, they can result in the droplet's shell fracturing and ejecting small ice fragments. These fragments act as secondary ice particles, which can continue to grow and multiply in the cloud.

Laboratory studies (Mason and Maybank, 1960; Pruppacher, 1967; Johnson and Hallett, 1968; Bader et al., 1974; Pruppacher and Schlamp, 1975) observed shattering of drops during freezing.

4.3 Precipitation formation

Warm rain process

The *warm rain process* is the production of rain at all levels above 0°C by the collision-coalescence of liquid particles (cloud droplet, drizzle drop and raindrop). The warm rain process involves the growth of liquid particles by *collision-coalescence*, and the growth is impeded by droplet breakup.

Additionally, this process can produce supercooled raindrops that freeze and form graupel, essential for glaciating convective tops by generating secondary ice crystals. In thunderstorms, the warm rain process converts condensed water into precipitable water (as drizzle droplets and raindrops) through collision-coalescence (Gao et al., 2021). In tropical and midlatitude regions, the warm rain process is significant for shallow and convective clouds (Lau and Wu, 2003; Kodama et al., 2009; Qin and Fu, 2016). The warm rain process is affected by aerosol loading and properties and, therefore, is essential for aerosol-cloud interactions (Rosenfeld et al., 2008; Stevens and Feingold, 2009; Dagan et al., 2015; Khain et al., 2015).

Cold rain process

Ice crystals in clouds form snow by aggregating and riming processes. Aggregation is the process by which ice crystals collide and stick together, forming larger snowflakes. Riming is a growth process in which supercooled water droplets collide with ice crystals and freeze onto their surfaces, leading to the formation of a layer of ice (Rogers and Yau, 1996; Khain and Pinsky, 2018b). Snow can rime to produce graupel. Hail is formed from the prolonged riming of ice crystals. Melting of graupel and hail below freezing levels can lead to the formation of cold rain. Cold precipitation contributes almost half of the global surface precipitation and plays a significant role in

both tropical and mid-latitude regions (Field and Heymsfield, 2015). Ice crystals can also grow through the Wegener-Bergeron-Findeisen (WBF) process (Wegener, 1912; Findeisen, 1938; Findeisen et al., 2015; Storelvmo and Tan, 2015), where the vapour pressure inside mixed-phase clouds falls between the saturation vapour pressures over ice and water surfaces. This allows ice particles to gain mass rapidly at the expense of supercooled droplets through deposition transfer.

Chapter 3

Aims and Scientific Hypotheses

Sect. 2 discusses the importance of representing cloud parameterization with known sources and sinks in a global model. Aerosol-cloud interactions are essential to define, and the cloud microphysical processes that predict the liquid and ice phases are also necessary. Correctly predicting the phase of the clouds is crucial since it can affect the radiation. These feedback processes motivate us to provide a more realistic representation of these cloud processes in the model.

This study aims to improve the processes and mechanisms that govern the formation and evolution of clouds using the CESM model. The thesis is divided into successive steps with implementations of the new microphysics in the model, and the valuations of the simulations are conducted, where each step aims to address a challenge.

1 Hypotheses

The following hypotheses will be either proven/disproven in this thesis.

1. SIP mechanisms can contribute to form ice number concentrations comparable to the observed values in convective clouds. The intensity of these SIP mechanisms varies, and these intensities are affected by environmental changes.
2. Time-dependence of INP freezing acts as a source for continuous ice nucleation and can increase the activity of INPs by a factor of about 2 (Jakobsson et al., 2022). For deep convective clouds, SIP and time-dependent INP activity contribute to the ice number concentrations.

3. Ice multiplication can dampen the impact of altering INPs and is always present when there is some precipitation.
4. Precipitation in clouds is formed from warm and cold rain processes. In deep convective clouds, the majority of the contribution to surface precipitation is from the cold rain processes.

The hypotheses will be evaluated with simulations using the new cloud scheme presented in the thesis and simulations from the Aerosol-cloud (AC) model.

2 Objectives

1. Implement the convective cloud microphysics scheme based on treatment in the high-resolution aerosol cloud model (Phillips et al., 2007, 2009, 2015, 2017a,b, 2018, 2020) in the SCAM6 version of the global model. Validate the predicted cloud properties against observational data for a convective storm in Oklahoma to assess the accuracy and reliability of the model in single-column mode.
 - (a) Assess and quantify the role of aerosols in activating cloud droplets and cloud-ice.
 - (b) Evaluate SIP processes with tagging tracers after including the overlooked representations in the cloud scheme.
2. Quantify the impact on the activity of SIP mechanisms from varying cloud-top temperatures.
 - (a) Evolution of the SIP mechanism and its dependency on time and cloud-top temperature
3. Elucidate the contribution of the warm rain and ice crystal process to the overall precipitation in the simulated mesoscale convective system.
4. Implement the stratiform cloud microphysics scheme and harmonize it with the new convection microphysics scheme (e.g., dealing with convective outflow). The predicted cloud properties were validated against observational data.
 - (a) Evaluating the role of aerosols in activating cloud particles and the role of overlooked SIP mechanisms.

Chapter 4

Methods

1 Community Earth System Model and Single Column Atmospheric Model, version6

CESM is a fully coupled global model with components for land, atmosphere, ocean, and sea-ice and is utilized to simulate future climate scenarios. The model's components provide feedback to each other, representing the complex processes of the Earth system. The Community Atmosphere Model, version 6 simulates the atmospheric conditions, radiative forcing, cloud processes and dynamics of the atmosphere. Single Column Model (SCM)s have a single vertical column of atmosphere that uses the same physical parameterization as the CESM to resolve the subgrid-scale processes. SCMs are good for model code development since they provide faster debugging and error identification.

SCAM6 is SCM version of the atmospheric component of CESM. SCAM6 utilizes the extensive CAM6 physics package but simplifies the representation of the resolved flow on a large scale. It simulates a single column and prescribes the large-scale flow and related tendencies from either observations or a simulation. This setup is valuable for studying parameterized physics behaviour without feedback involving large-scale circulation. It is useful for parameterization development and understanding physical processes within prescribed large-scale circulation constraints.

The clouds are represented as stratiform and convective clouds in the CAM6 physics. The stratiform scheme by Morrison and Gettelman (2008) and convective scheme by Zhang and McFarlane (1995); Song and Zhang (2011) are represented in the model.

1.1 Convection Scheme

In CAM6, the convection scheme is represented by Zhang and McFarlane (1995), hereafter as ZM and the convection microphysics scheme by Song and Zhang (2011), hereafter as SZ11 scheme.

ZM scheme was modified to include a new detrainment formulation based on Bechtold et al. (2008) and Derbyshire et al. (2011) to represent turbulent detrainment and organized detrainment, respectively.

A "new aerosol-cloud convection (ACC)" parameterization is implemented, which replaces the SZ11 scheme. ACC is a two-moment hybrid bin/bulk scheme based on the cloud microphysics of high-resolution 3-D cloud model (Phillips et al., 2007, 2009, 2017a, 2018; Kudzotsa et al., 2016).

The approach was to implement a buoyancy-driven Lagrangian air parcel in the bulk plume. The cloud properties of the parcel are representative of all the deep convective clouds in the grid box. The air parcel is integrated numerically, and there is no numerical diffusion. The ascent of the parcel is determined by the vertical velocity. The parcel ascends from the base of the plume to the convective top.

The initial vapour mixing ratio of the parcel is set to the environmental value. The initial vertical velocity is set to 0.4 m/s. The temperature and pressure of the air parcel follow that of the bulk plume. The air parcel is lifted vertically with a time step of 0.025 seconds.

Vertical velocity

The vertical velocity ($w_{up}(z)$) is calculated by integrating the kinetic energy vertical gradient as done by Simpson and Wiggert (1969). The vertical velocity of the parcel is dependent on the temperature, weight of the condensate (cloud liquid, rain, cloud ice, graupel, snow), gravity, momentum drag, and entrainment/detrainment mass flux of the environment.

Evolution of cloud hydrometeors and aerosols

The continuous entrainment equations are numerically integrated with a fine timestep of 0.025 s.

$$\frac{DX_{cld}}{Dt} = -E_u(X_{cld} - X_{env}) + \sum S_{X_{cld}} \quad (4.1)$$

Here X_{cld} is any conserved variable such as mass and number mixing ratio of cloud liquid, cloud ice, rain, snow, graupel and actual number mixing ratio for each size bin of the aerosols in any given chemical species (sulphate, dust, sea salt,). E_u is the entrainment rate, and $S_{X_{cld}}$ are source/sink terms.

Tagging tracers

The components of cloud liquid, which is initiated from the in-cloud activation, and also the components of cloud-ice initiated from different primary and SIP processes are traced and analyzed. These components are passive and do not interact with the microphysics.

Aerosol treatment

Seven chemical species (sulphate, dust, sea salt, black carbon, soluble organics, primary biological matter, and non-biological insoluble organics) are represented in the global model. A lognormal aerosol size distribution over the model height is used to represent the aerosol species given by Phillips et al. (2009) with distribution parameters of each mode (geometric mean size, spectral width, ratio of total numbers between multiple modes) being constrained by observations. During the ascent, the continuous entrainment equation is solved for each bin of the aerosols present in the environment and in the parcel. The aerosols are classified into two main categories: soluble and solid aerosols.

- The soluble aerosol species are ammonium sulphate (its bi-modal distribution is separated into two independent modes as SO_41 and SO_42), sea-salt and soluble organics.
- The insoluble aerosol species comprises mineral dust, black carbon, insoluble non-biological organic, primary biological matter and non-biological insoluble organics

Cloud microphysics

The ACC scheme is a hybrid bin/bulk scheme. Bulk microphysics is utilized for the representation of advection and sedimentation of cloud hydrometeor. The bin microphysics is used for the processes of coagulation and growth processes.

The cloud hydrometeors represented in the ACC scheme are mass and number mixing ratios of cloud liquid, rain, cloud-ice, graupel and snow. The bulk parameterization for cloud hydrometeors is represented by a γ -distribution following Phillips et al. (2007).

Initiation of cloud hydrometeors

Cloud droplet activation The cloud droplets are activated at the cloud-base and in-cloud when supersaturation is positive. Soluble aerosol species activate cloud droplets at the cloud-base. Ming et al. (2006) scheme explicitly links the chemistry and size distribution of aerosols, vertical velocity and CDNC. In-cloud the droplets can be initiated by soluble and coated solid aerosols following the κ -Kohler theory (Petters and Kreidenweis, 2007).

Heterogeneous nucleation of cloud-ice Empirical parameterization (EP) developed by Phillips et al. (2008, 2013) is implemented. EP treats four modes of heterogeneous nucleations: deposition, condensation, and immersion. EP relies on the surface area and chemistry of INP, with a threshold of size greater than $0.1\mu\text{m}$. EP is based on INP activity from Continuous Flow Diffusion Chamber (CFDC) measurements of during the Ice Nuclei Spectroscopy (INSPECT) campaigns (DeMott et al., 2003). Jakobsson et al. (2022) performed isothermal experiments for immersed INPs over many hours to quantify the time-dependent freezing of INPs. EP is modified to include the temperature shift of the INPs following the method proposed by Jakobsson et al. (2022). According to Jakobsson et al. (2022),

$$\Delta\tilde{T}_X = -A_X\tilde{t}^{-\beta_X} \quad (4.2)$$

A_X and β_X are the fitting constants corresponding to subscript X and the values are provided in the Jakobsson et al. (2022, Table 6).

Homogeneous freezing of cloud droplets The supercooled droplets instantaneously freeze at about -35° – -37°C according to the size (Phillips et al., 2007, 2009). Larger droplets freeze first based on the supersaturation and updraft velocity. The fraction of cloud droplets that evaporate without freezing due to vapour growth of frozen droplets causing subsaturation is represented with a lookup table.

Hallett Mossop process The HM process is active between the temperatures -3° to -8°C following Phillips et al. (2007) and Kudzotsa et al. (2016). It is assumed 350 splinters are produced for every milligram of liquid accreted onto snow and graupel.

Fragmentation during ice-ice collisions It follows Phillips et al. (2017a) based on the energy conservation of colliding particles to determine the number of secondary fragments produced. Bin microphysics is utilized in this formulation. The number and mass mixing ratios of the two colliding ice particles are discretised into 33 size bins. The permutations of all combinations of the size bins, ice morphology, collision kinetic energy (CKE) are considered in the formulation.

Fragmentation during raindrop freezing This follows the formulation developed by Phillips et al. (2018). This formulation uses the bin scheme to represent all the permutations of the interaction between the supercooled raindrops and ice particles. Two modes of fragmentation during raindrop freezing are treated,

1. Mode 1 : ice fragments are produced when supercooled raindrop (size between 0.05-5 mm) collides with a smaller ice particle or an immersed INP freezes it heterogeneously.
2. Mode 2 : ice fragments are produced when supercooled raindrop collides with a larger ice particle.

Growth of cloud hydrometeors

Condensational growth of cloud droplets Cloud droplets grow by condensation following the Rogers and Yau (1996, Eqs. 9.4 and 7.18). Emulated bin microphysics is implemented to calculate the growth rate in each size bin.

Vapour growth of ice The growth rate follows Rogers and Yau (1996, their Eq. 9.4) using the emulated bin approach. The growth rate is determined for each size bin and then summed over the entire bin system to get the bulk number and mass mixing ratios.

Autoconversion of cloud droplet to raindrop This follows Kogan (2013) using the bulk scheme.

Autoconversion of cloud-ice to snow The formulation developed by Schoenberg Ferrier (1994) and Kudzotsa et al. (2016) is implemented with the bulk scheme approach.

Table 4.1: The microphysical conversion tendencies for mass mixing ratio ($\text{kg}^{-1}\text{kg}^{-1}\text{s}^{-1}$). The first symbols within the parentheses before the semicolon represent the final species in each interaction. The symbols after the semicolon represent the interacting species. The table is a modified version of Phillips et al. (2007, Table 1.).

Symbol	Meaning
Ac ($q_r; q_c q_r$)	Accretion of cloud droplets by rain
Ac ($q_g, q_i; q_c q_i$)	Riming of cloud droplet by cloud-ice
Ac ($q_g, q_i; q_g q_c$)	Riming of cloud droplet by graupel/hail
Ac ($q_s, q_i; q_s q_c$)	Riming of cloud droplet by snow
Ac ($q_c, q_r, q_i, q_g; q_r q_g$)	Accretion of rain by graupel/hail. Fragments of cloud-ice fragments and splashes are produced
Ac ($q_s; q_i q_s$)	Accretion of cloud-ice by snow
Ac ($q_c, q_s, q_g, q_i; q_s q_r$)	Accretion of snow by rain
Ac ($q_g, q_i; q_i q_r$)	Accretion of cloud-ice by rain
Ag ($; q_i q_i$)	Aggregation of cloud-ice and cloud-ice
Ag ($q_i; q_s q_s$)	Aggregation of snow and snow. Fragments of cloud-ice are produced
Ag ($q_i; q_g q_g$)	Aggregation of graupel/hail and graupel/hail. Fragments of cloud-ice are produced
Ag ($q_g, q_s, q_i; q_g q_s$)	Aggregation of graupel/hail and snow. Fragments of cloud-ice are produced
Ag ($q_g, q_i; q_g q_i$)	Aggregation of graupel/hail and cloud-ice. Fragments of cloud-ice are produced

Autoconversion of snow to graupel Graupel/hail is formed by riming of snow using a bin scheme approach (Phillips et al., 2017b). The riming rate is determined following Gautam Martanda (2022).

Accretion, riming and aggregation processes The precipitation in the air parcel grows by the interactions between particles (accretion, riming and aggregation). The different combinations of the interactions included in the model are shown in Table 4.1. The accretion of cloud liquid by rain is treated using the bulk parameterization following Kogan (2013). All the other processes in Table 4.1 are treated using the emulated bin approach.

Sedimentation of cloud hydrometeors Bulk microphysical formulae are used to number and mass-weighted fall velocities of rain, and an emulated bin approach is used for graupel/hail. The fall velocities of graupel/hail depend on the density and ice morphology.

1.2 Stratiform scheme

In CAM6, the stratiform scheme is represented by Morrison and Gettelman (2008), hereafter as MG08. The study modified the stratiform scheme to include new microphysical formulations. This work involved modifying the existing scheme. The following modifications were made to the stratiform scheme

1. Cloud base droplet activation follows Ming et al. (2006) (sect. 1.1).
2. Heterogeneous ice nucleation is represented by EP (sect. 1.1).
3. Homogeneous freezing of supercooled droplets follows Phillips et al. (2007, 2009).
4. Graupel/hail is added during the microphysical conversion processes. The mass and number mixing ratio of snow is divided into two categories: snow and graupel/hail, according to a lookup table. Since graupel is not a prognostic variable in the model, the graupel tendencies are added to the snow tendencies for advection into the large-scale model grid.
5. The accretion of cloud liquid by rain is not changed. Otherwise, all the growth processes of accretion, aggregation and riming in Table 4.1 are added in the stratiform scheme (sect. 1.1).
6. The stratiform scheme now represents 3 SIP mechanisms: HM process (sect.1.1, fragmentation during ice-ice collisions (sect.1.1) and fragmentation during rain-drop fragmentation (sect.1.1).

The warm rain process, WBF process and heterogeneous freezing of rain have not been modified and are used as is when doing the simulations. The modified version of the MG08 scheme is referred to as the LLS24 scheme.

2 Analysis of the role of time-dependent freezing of INPs

The role of time-dependent freezing of immersed INPs was studied. Jakobsson et al. (2022) proposed a temperature shift approach to implement time-dependent freezing in numerical models. This approach was implemented in EP.

The temperature shift is given by,

$$\Delta T_X(\tilde{t}) = -A_X \tilde{t}^{-\beta_X} \quad (4.3)$$

Jakobsson et al. (2022, Table 6) provided the values of the fitting constants A_X and β_X subscript X

\tilde{t} is the time of the parcel since entering the cold parts of the cloud. The exponential decay of a passive tracer (Q) with time determines \tilde{t} . The evolution of the passive tracer Q is given as,

$$\frac{DQ}{Dt} = \begin{cases} -Q/\tau_Q, & T < 0^\circ\text{C and IWC} > 10^{-6} \text{ kg m}^{-3}. \\ 0 \text{ kg m}^{-3}, & \text{otherwise.} \end{cases} \quad (4.4)$$

$Q = Q_0 = 1 \text{ kg}^{-1}$, everywhere outside the glaciated part of the cloud, both in the environment and the parcel. $\tau_Q = 1800 \text{ s}$ is an arbitrary relaxation time. The analytical solution of the Eq. 4.4 is given as

$$\tilde{t} \approx -\tau_Q \ln(Q/Q_0) \quad (4.5)$$

3 Aerosol-cloud (AC) model

AC model uses the general framework of the Weather Research and Forecasting (WRF) model with a hybrid bin/bulk spectral microphysics scheme (Phillips et al., 2007, 2009, 2013, 2015, 2017a,b, 2020). AC uses a double-moment approach to represent cloud hydrometeors. It represents cloud droplets, rain, snow and graupel/hail as prognostic variables. AC represents eight aerosols species, mineral dust, black carbon, sea-salt, insoluble organics, sulphates in two independent modes, soluble organics and Primary Biological Aerosol Particles (PBAPs).

4 Mid-latitude Continental Convective Clouds Experiment (MC3E) Campaign

The Mid-latitude Continental Convective Clouds Experiment (MC3E) campaign was carried over Oklahoma from April to June 2011. The Central Facility (CF) was located at 36.695° N and 97.485° W with 20 extended facilities. The field campaign incorporated a comprehensive sounding array, remote sensing, and in situ aircraft observations, along with National Aeronautics and Space Administration (NASA) Global precipitation measurement (GPM) ground validation remote sensors (Jensen et al., 2016).

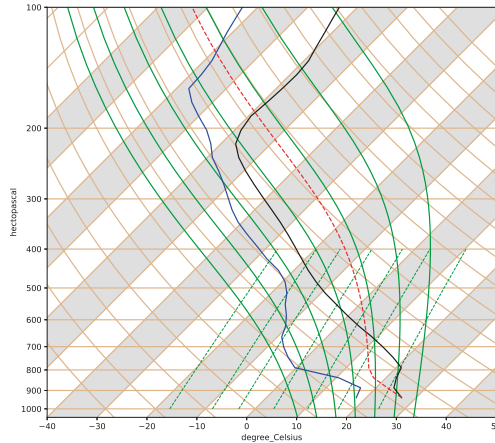


Figure 4.1: A Skew-T Log-P diagram showing the atmospheric profiles of temperature (solid black line), dew point temperature (solid blue line) for the initial simulation time of 00 UTC on 10 May 2011

4.1 11 May 2011 mesoscale convective system.

A surface cold front initiated organized severe convection as it moved across the Texas-Oklahoma panhandle. The mesoscale convective system (MCS) was moving northeast with a stratiform precipitation region located north of it. The MCS had already matured and transitioned to a trailing stratiform region as it passed over the CF.

Figure 4.1 shows the vertical profiles of air and dew point temperature at 00 UTC on 10 May 2011. The wind speed was intense for the depth of the atmosphere (~ 10 m/s). Figure 4.1 shows the Lifting condensation level (LCL) is at 827 hPa.

4.2 Airborne measurement

National Aeronautics and Space Administration (NASA) ER-2 and the University of North Dakota (UND) Cessna Citation II aircraft sampled the MCS system. The Citation II sampled the weaker stratiform region in coordination with the ground facilities. The Citation II carried the meteorological instruments described in Table 4.2, and its focus was to sample the ice-phase hydrometeor at altitudes of $\sim 4 - 13$ km.

Table 4.2: Meteorological instruments carried on Citation II aircraft

Instrument	Range
Cloud Imaging Probe (CIP)	0.025 – 1.5 mm
2D Cloud imaging probe (2DC)	0.03 – 1.0 mm
High-volume precipitation spectrometer, version 3 (HVPS-3)	0.15 – 19.2 mm
Cloud droplet probe (CDP)	2 – 50 μm
King hot-wire Liquid water content probe	0.01 – 5 g m^{-3}
Nevzorov probe	0.03 – 3 g m^{-3}

2DC and HVPS-3 probe had anti-shatter tips, while CIP did not have them. Field et al. (2006) introduced a method to minimize the effect of shattered ice on the probes. This method of considering ice particles with sizes $> 200\mu\text{m}$ is implemented in analysing the aircraft data to remove the shattered particles.

4.3 Ground based observation

The MC3E campaign consisted of 20 central facilities, which covered an area of about 150km. The spatial variability of moisture, surface fluxes, momentum, temperature, humidity, and wind properties were measured by the radiosonde array (Jensen et al., 2016). Xie et al. (2014) used the constrained variational analysis approach to obtain large-scale forcing, surface heat, and moisture.

Chapter 5

Results

1 Implementation of new convective microphysics

The new convective parameterization, referred to as *ACC*, was implemented in the model. Simulations were carried out to study an observed case of the MC3E storm on 11 May 2011, comparing the performance of the new scheme with that of the original unmodified version. Comparing the simulation results in SCAM6 with observations reveals that the *ACC* scheme effectively reproduces key characteristics of the storm. The *ACC_24* simulations included the new *ACC* convection microphysics scheme and the original MG08 stratiform scheme. SZ11 simulations included the original deep convective microphysics by Song and Zhang (2011) and the original MG08 stratiform scheme.

Figure 5.1a shows that the predicted cloud droplet number concentration (CDNC) at 14°C and -28°C differs by 10% from the observations. Also, around -10°C , where observations are present, *ACC_24* accurately predicts CDNC. At cloudbase, SZ11 underpredicts CDNC by an order of magnitude. Above the cloud base, the predicted CDNC values differ from observations up to a factor of 10 for the SZ11 run.

Figure 5.1b shows that the liquid water content (LWC) agrees well with the observations at the cloud base, reaching a maximum of 1.6 gm^{-3} near the freezing level. The discrepancy between predicted LWC by *ACC_24* and the observation is less than a factor of 2. However, at -11°C , where most observations are present, the SZ11 scheme predicts levels higher than those observed by a factor of 3. Additionally, SZ11 forecasts cloud liquid above the homogeneous freezing level.

The vertical velocities predicted by the SZ11 attain a maximum of 5 m/s at a homogen-

eous freezing level. However, the ACC_24 run predicts a maximum vertical velocity of 15 m/s at -15°C .

In Figures 5.1d and e, the filtered ice particle concentrations have been plotted to avoid the shattering bias. ACC_24 performs better in predicting ice particle concentration compared to the SZ11 run. The predicted total ice particle concentration for particles larger than 0.2 mm closely matches the observed data, except at -10°C and -11°C levels, where it differs by a factor of about 10 from observations. However, at -15°C , the results from ACC_24 run align well with the observed data. Ice particles are absent below the -15° for the SZ11 run.

Figure 1b predicted that the total ice particle number concentration for ice particles with sizes greater than 1mm is of the same order as the observations at all levels where observations are present. The predicted total ice particle concentrations differ from the observations by about a factor of 4 or 5.

ACC_24 and SZ11 runs are able to predict the two precipitation peaks (Figure 5.1f). For the stronger peak, ACC_24 overestimated the precipitation about 40% more than the observed peak, and SZ11 underestimates the second peak, which is about 79% of the observed value. ACC_24 run predicts higher intensity than the observations for the first peak, and the SZ11 run predicts the intensity accurately.

Figure 5.1g shows that accumulated precipitation at the end of the simulation for the ACC_24 run is 6mm more than observed value and for the SZ11 run underpredicts by 5mm.

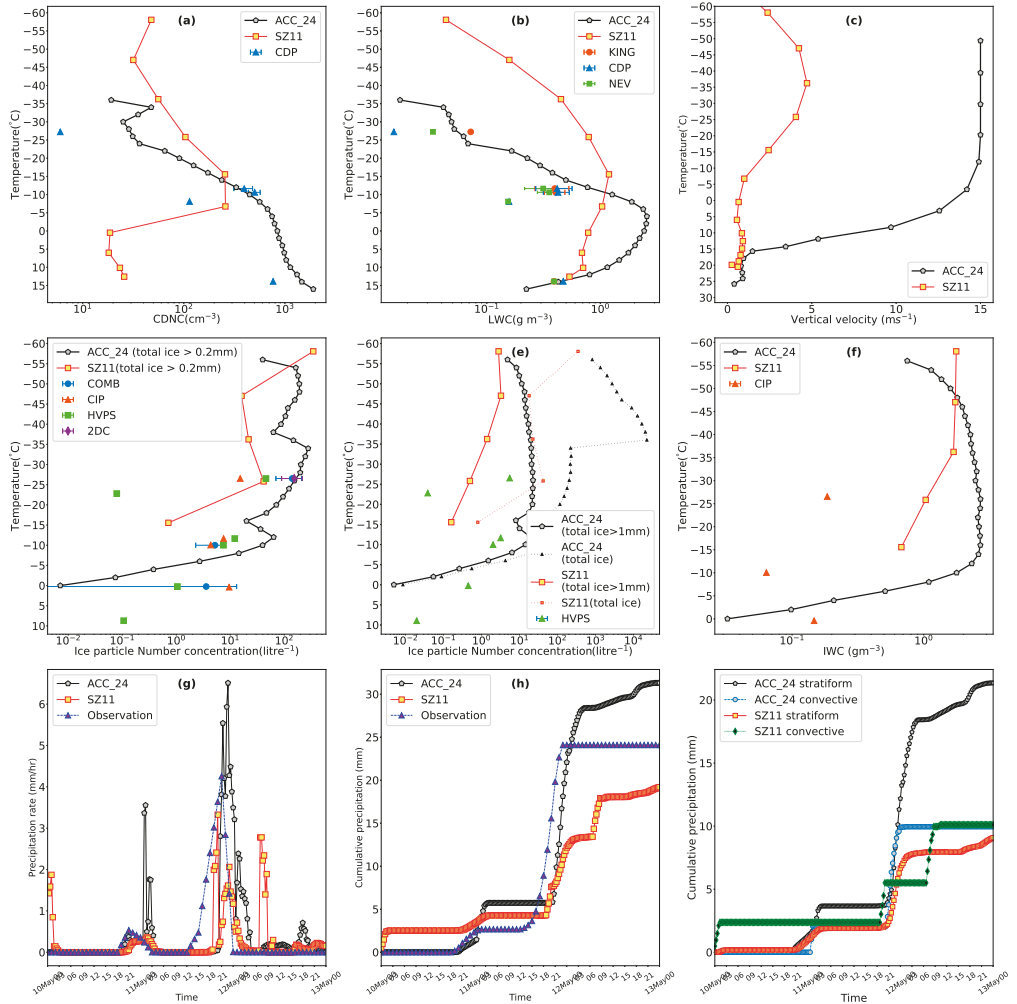


Figure 5.1: Predicted (a) CDNC compared with CDP probe data, (b) LWC compared with CDP, KING and Nevzorov probe data, (c) vertical velocity, (d) total number concentration of ice particles with sizes greater than 0.2mm compared with 2DC, CIP, HVPS-3 probe data and COMB data, (e) total ice number concentrations of ice particles with size greater than 1 mm compared HVPS-3 probe data (f) total ice particle mass mixing ratio from the SZ11 (solid red line with square) and ACC (solid black line with pentagram) simulations. The cloud microphysical properties are conditionally averaged over cloudy convective updrafts ($w_{up} > 3 \text{ m s}^{-1}$). Predicted (g) precipitation rate mm/hr and (h) accumulated surface precipitation compared with observations (Xie et al., 2014). Predicted (i) stratiform and convective cumulative precipitation from the SZ11 and ACC_24 simulations.

1.1 SIP mechanisms

The mass and number concentration of cloud-ice initiated from each process, heterogeneous nucleation, homogeneous freezing and secondary ice process are tracked using passive prognostic variables. The tagging tracer does not alter the cloud properties.

The results from the tagging tracers, which represent the total cloud-ice concentrations from the different sources, are conditionally averaged over convective clouds ($w_{up} > 3 \text{ m s}^{-1}$) and are plotted in Fig. 5.2.

Figure 5.2a shows fragmentation during ice-ice collision is the most productive and contributes up to 99% of the total cloud-ice in mixed-phase regions. HM process is predicted to be active in the region -3 and -8°C level, but the splinters generated are not high compared to other processes. The raindrop freezing fragmentation is also less active than the other two SIP mechanisms. At -36°C level, 99% of cloud-ice generated is from homogeneous freezing of supercooled droplets.

Figure 5.2c shows heterogeneous ice nucleation, SIP mechanisms, and homogeneous freezing contribute 1%, 6%, 93% respectively to the total budget of cloud-ice initiated. Figure 5.2d shows fragmentation during ice-ice collision mechanism contributes the most to the mass mixing ratio of cloud-ice initiated.

Figure 5.2c and e show that cloud-ice contributes the most to the ice particle number concentrations. Cloud-ice, snow and graupel contribute 98%, 1.5% and 0.2%, respectively, to the total ice particles initiated. The mass budget shows graupel/hail and snow are the significant contributors to the total mass of ice particles initiated.

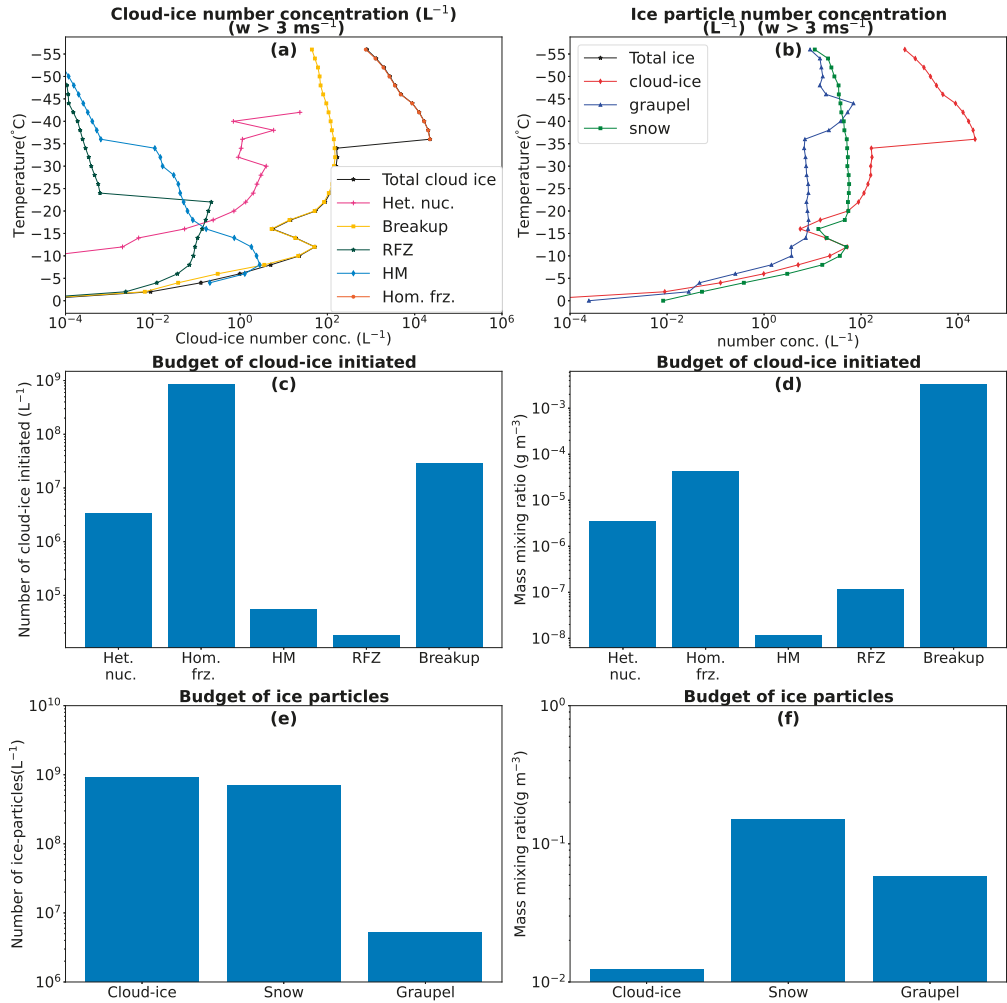


Figure 5.2: (a) Comparison of the predicted total number of cloud-ice from the SIP mechanism in the simulation compared with predicted total cloud-ice. (b) The contributions from cloud-ice (dotted line with diamond), graupel/hail (dotted line with triangle) and snow (dotted line with square) are plotted, as well as total ice (solid line with pentagram). Bar plot for the (c) budgets of the number of cloud-ice particles and (d) budget of the mass mixing ratio of cloud-ice particles initiated from heterogeneous ice nucleation ('Het. nuc.'), homogeneous freezing ('Hom. frz.'), fragmentation during ice-ice collisions ('Breakup'), fragmentation during raindrop freezing ('Rfz') and HM process. Bar plot of the (d) budgets of the number and (e) budget of the mass mixing ratio of cloud-ice, snow and graupel particles initiated in the cloud for the ACC_24 simulation. The cloud microphysical properties are conditionally averaged over cloudy convective updrafts ($w_{up} > 3 \text{ m s}^{-1}$).

1.2 Soluble aerosol species in environment

The concentrations of the soluble aerosol species were changed in the environment using a height-dependent factor. For the high-CCN case, the factor decreases from 10 at the ground to unity at 11km. For the low-CCN case, the factor increases from 0.1 to

unity at 11 km. The changes in the aerosol concentrations were done to represent the contrast between polluted and maritime aerosol conditions.

Figure 5.3a depicts that in the low-CCN run, there is a higher average cloud droplet diameter with a maximum of $24\mu\text{m}$ compared to the high-CCN scenario, with an average cloud droplet diameter reaching only $10\mu\text{m}$.

Figure 5.3b shows an increase in LWC at Cloudbase by a factor of 2 and a decrease by a factor of 6 for high-CCN and low-CCN run, respectively. Below the freezing level, the LWC for low-CCN and high-CCN closely follow the ACC_24 run.

Figure 5.3c shows that at cloudbase, CDNC is increased and reduced by a factor of 3 relative to ACC_24 for high-CCN and low-CCN runs, respectively.

Figures 5.3e and f shows that in all three runs, almost 99% of ice particles are initiated by breakup during ice-ice collisions. In mixed-phase areas, the ice particle number concentrations are increased and decreased by a factor of 2 compared to ACC_24 run for high-CCN and low-CCN run, respectively. Above the mixed phase regions, the ice concentrations for the high-CCN case are increased by an order of magnitude and by a factor of 2 for the low-CCN case compared to the ACC_24 run because of the increased CDNC aloft (Figure 5.3).

The budget indicates that in the low-CCN scenario, there is a higher activity of HM (3 times) and raindrop freezing fragmentation (5 times) compared to the ACC24 run. Additionally, snow and graupel budgets show a relative increase by a factor of 4 and 2, respectively, compared to the ACC24 run, resulting from an enhanced riming process promoted by abundant supercooled cloud liquid aloft.

The accumulated surface precipitation at the end of the simulation for the Low-CCN run is decreased by 15% compared to ACC_24 due to the depletion of snow by accretion onto supercooled rain and graupel (Figure 5.3e). The high-CCN run shows an increase in the cumulative precipitation by 3% because of the prevalence of the ice crystal process to produce precipitation.

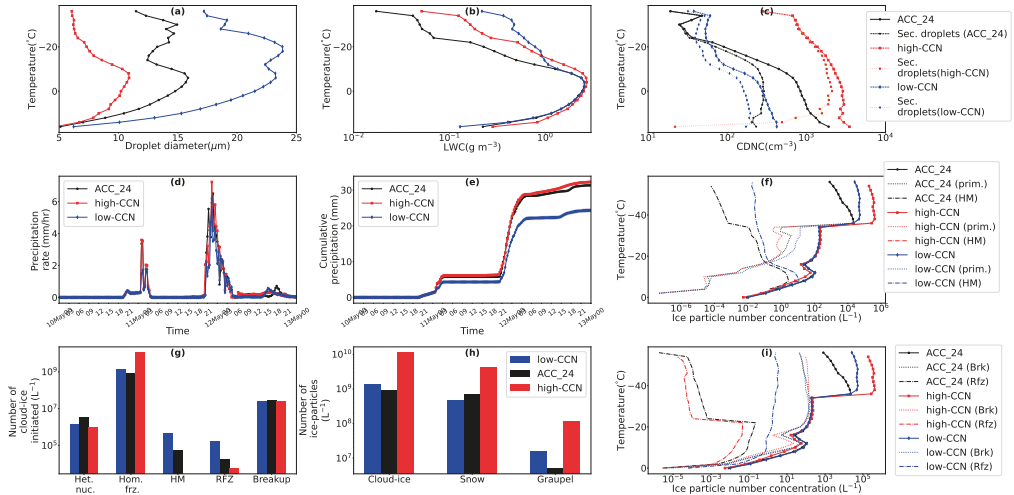


Figure 5.3: Vertical profiles of predicted (a) mean cloud droplet diameter, (b) LWC and (c) CDNC plotted with secondary droplets, (d) surface precipitation rate (mm hr^{-1}), (e) cumulative surface precipitation (mm) and (f) total ice particle number concentration with tagging tracers for cloud-ice initiated from primary ice processes ('prim.') (dotted line), HM process (dash-dotted line), and (i) total ice particle number concentration with tagging tracers for cloud-ice initiated from breakup in ice-ice collisions ('Brk') (dotted line), raindrop freezing fragmentation process ('Rfz') (dashdotted line) from the high-CCN (solid red line with squares), low-CCN (solid blue line with diamond) and ACC_24 (solid black line with pentagram) simulations. The cloud microphysical properties are conditionally averaged over cloudy convective updrafts ($w_{up} > 3 \text{ m s}^{-1}$). Bar plot for the (g) budgets of the number of cloud-ice particles initiated from heterogeneous ice nucleation ('Het. nuc.'), homogeneous freezing ('Hom. frz.'), breakup in ice-ice collisions ('Breakup'), raindrop freezing fragmentation ('Rfz') and HM process and (h) budgets of the number of cloud-ice, snow and graupel particles initiated in the cloud for the ACC_24 (black coloured bars), high-CCN (red coloured bars) and low-CCN (blue coloured bars) simulations.

1.3 Solid aerosol species in the environment

The concentrations of the solid aerosol species were changed in the environment using a height-dependent factor. For the high-INP case, the factor decreases from 10 at the ground to unity at 11km. For the low-INP case, the factor increases from 0.1 to unity at 11 km. The changes in the aerosol concentrations were done to represent the contrast between polluted and maritime aerosol conditions.

Figure 5.4a illustrates a pattern of reduction in average droplet size as the solid aerosol loading increases, reaching a peak of $12 \mu\text{m}$ in the high-INP scenario. The mean droplet size remains relatively unchanged for the low-INP case, with only a slight increase of $0.5 \mu\text{m}$ compared to ACC_24.

Figure 5.4b shows that in the low-INP run, the LWC does not show much change from the ACC_24. In the high-INP run above -10 degree C, LWC increases by up to 60% compared to ACC_24. In Figure 5.4c, the CDNC at cloud-base is reduced by a factor of 2 for the high-INP case compared to ACC_24 and reduced by 30% for the low-INP

case. The CDNC profiles for the low-INP scenario closely resemble those of ACC_24.

Figure 5.4f shows that in the mixed-phase regions, both low- and high-INP runs shows a similar profile as the ACC_24 run with only a slight increase by a factor of 2 from ACC_24 to the high-INP case.

Figure 5.4g shows the budget for cloud-ice initiated by heterogeneous nucleation is increased by a factor of 3 and is reduced by a factor of 6 compared to ACC_24 run for the low-INP run. The cloud-ice initiated from breakup in ice-ice collisions shows only a slight change by 2 from low-INP to the high-INP run, exceeding the cloud-ice initiated from heterogeneous nucleation by up to about an order of magnitude.

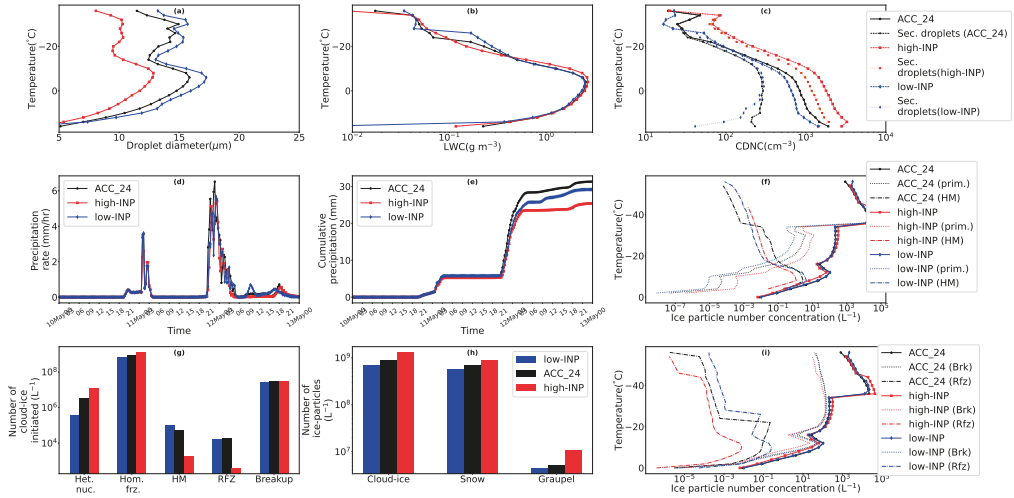


Figure 5.4: (a) Predicted mean cloud droplet diameter, (b) predicted LWC and (c) predicted CDNC plotted with secondary droplets, (d) surface precipitation rate (mm hr^{-1}), (e) cumulative surface precipitation (mm) and (f) total ice particle number concentration with tagging tracers from cloud-ice from primary ice processes ('prim.') (dotted line), HM process (dash-dotted line), and (i) total ice particle number concentration with tagging tracers from breakup in ice-ice collisions ('Brk') (dotted line), raindrop freezing fragmentation process ('Rfz') (dash-dotted line) from the high-INP (solid red line with squares), low-INP (solid blue line with diamond) and ACC_24 (solid black line with pentagram) simulations. The cloud microphysical properties are conditionally averaged over cloudy convective updrafts ($w_{up} > 3 \text{ m s}^{-1}$). Bar plot for the (g) budgets of the number of cloud-ice particles initiated from heterogeneous ice nucleation ('Het. nuc.'), homogeneous freezing ('Hom. frz.'), breakup in ice-ice collisions ('Breakup'), raindrop freezing fragmentation ('Rfz') and HM process and (h) budgets of the number of cloud-ice, snow and graupel particles initiated in the cloud for the ACC_24 (black coloured bars), high-INP (red coloured bars) and low-INP (blue coloured bars) simulations.

2 Analysis of the role of time-dependent freezing of INPs

The role of time-dependent freezing of immersed INPs was studied. Jakobsson et al. (2022) proposed a temperature shift approach to implement time-dependent freezing in EP. Simulations were conducted with the SCAM6 and AC models to evaluate the role

of time-dependent freezing on INP activity in the MC3E storm.

2.1 Results from SCAM6

ACC_24 are compared with the sensitivity simulation where the effect of time-dependence is included in EP. Figure 5.5 reveals that the cloud properties are unaffected when the time dependence is included. The tagging tracer for cloud-ice initiated by heterogeneous ice nucleation is plotted (Figure 5.5e), and it shows a change $<0.5\%$ compared to ACC_24 simulations.

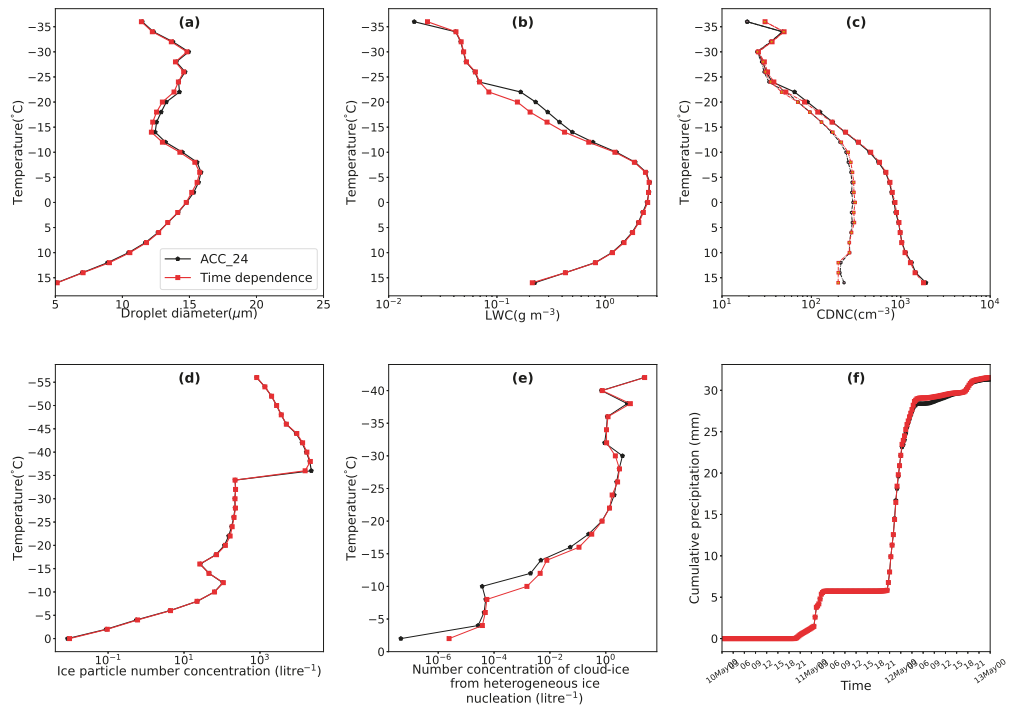


Figure 5.5: Predicted (a) mean cloud droplet diameter, (b) LWC, (c) CDNC, (d) total number concentration of ice particles, (e) tagging tracer representing the cloud-ice generated by Heterogeneous ice nucleation from the Time dependence (solid red line with square) and ACC_24 (solid black line with pentagram) simulations. The cloud microphysical properties conditionally averaged over cloudy convective updrafts ($w_{up} > 3 \text{ m s}^{-1}$). Predicted (f) cumulative surface precipitation from the Time dependence (solid red line with square) and ACC_24 (solid black line with pentagram) simulations are plotted.

2.2 Results from the AC model

Waman et al. (2023) simulated various cloud types using the AC model. Figures 5.6 show the number concentration of active INPs in the MC3E storm over stratiform re-

gions. Here, CTRL simulation includes the effect of time dependence, and NO_TDF simulation excludes this effect. The predicted active dust INPs are increased by a factor of 2 for the MC3E run. Waman et al. (2023) observed no significant changes in the total ice concentrations when they included the time-dependent effect.

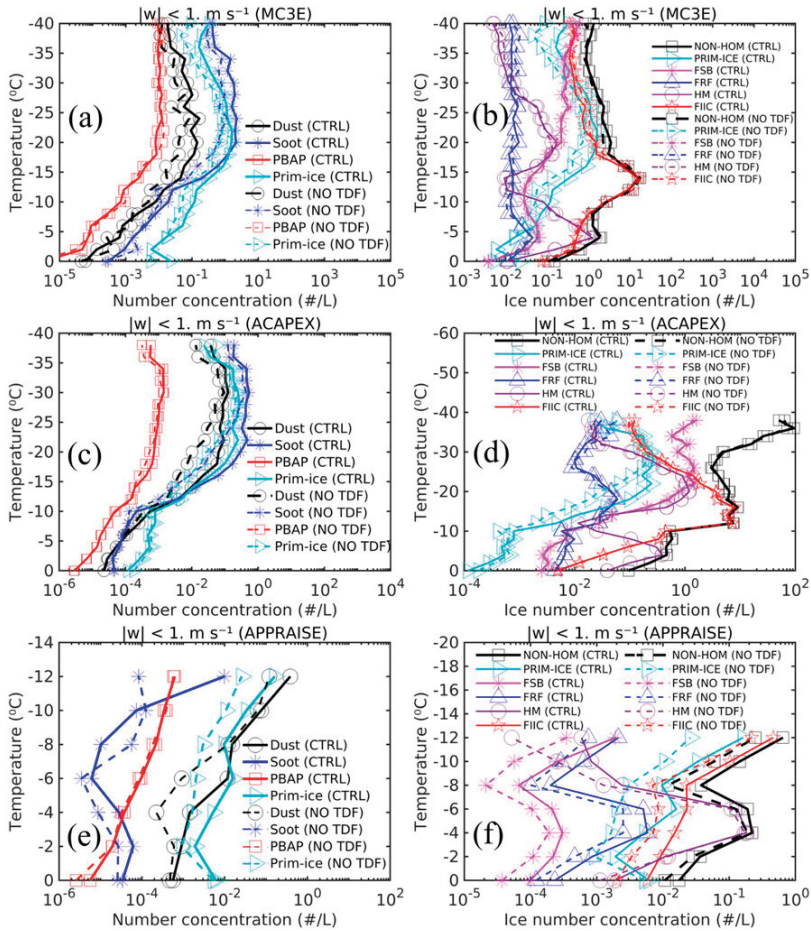


Figure 5.6: (left) The predicted number concentrations of active INPs conditionally averaged over stratiform regions ($|w| < 1$ m/s) from mineral dust (solid line with open circles), soot (solid line with asterisks), and PBAP (solid line with squares), and concentrations of heterogeneously nucleated ice (PRIM-ICE, forward-pointing triangles) for the (a) MC3E, (c) ACAPEX, and (e) APPRAISE cases. The same information is shown with dotted lines for the “no time-dependent INP” run. (right) The concentrations of total nonhomogeneous ice (total cloud ice and snow minus total homogeneous ice; solid line with squares) and various tracer terms defining SIP processes such as fragmentation during sublimation (FSB; solid line with asterisks), ice-ice collisions (FIC; solid line with pentagrams) and raindrop freezing (FRF; solid line with upward-pointing triangles), and the HM process (HM; solid line with open circles) for the (b) MC3E, (d) ACAPEX, and (f) APPRAISE case, respectively. The same information is shown with the dotted lines for the “no time-dependent INP” run. To compare the number concentrations of heterogeneously nucleated ice and total nonhomogeneous ice, heterogeneously nucleated ice (PRIM-ICE; forward-pointing triangles) is also shown in the right column. The figure is adapted from Waman et al. (2023).

3 Analysis of the warm and cold rain processes

Gupta et al. (2023) simulated three storm types using the AC model to study the contribution of the warm and cold rain processes to the surface precipitation.

- Warm-rain: raindrops are formed by collision-coalescence of cloud droplets. They may freeze to form ("warm") graupel, which may melt when falling.
- Cold-rain: ("cold") graupel/hail is formed by riming of ice crystals. ("cold") graupel might melt when falling.

Figures 5.7a show that mass mixing ratio of warm graupel is less than the cold-graupel by an order of magnitude. Figure 5.7b shows that the number mixing ratio of the cold graupel is less than the warm graupel by an order of magnitude. Below the freezing level, cold rain is more than the warm rain. Figures 5.7i and j show that for both convective and stratiform regions of the MC3E storm, the cold precipitation dominates the total precipitation. Gupta et al. (2023) predicts that stratiform precipitation contributes 80% of the total accumulated surface precipitation

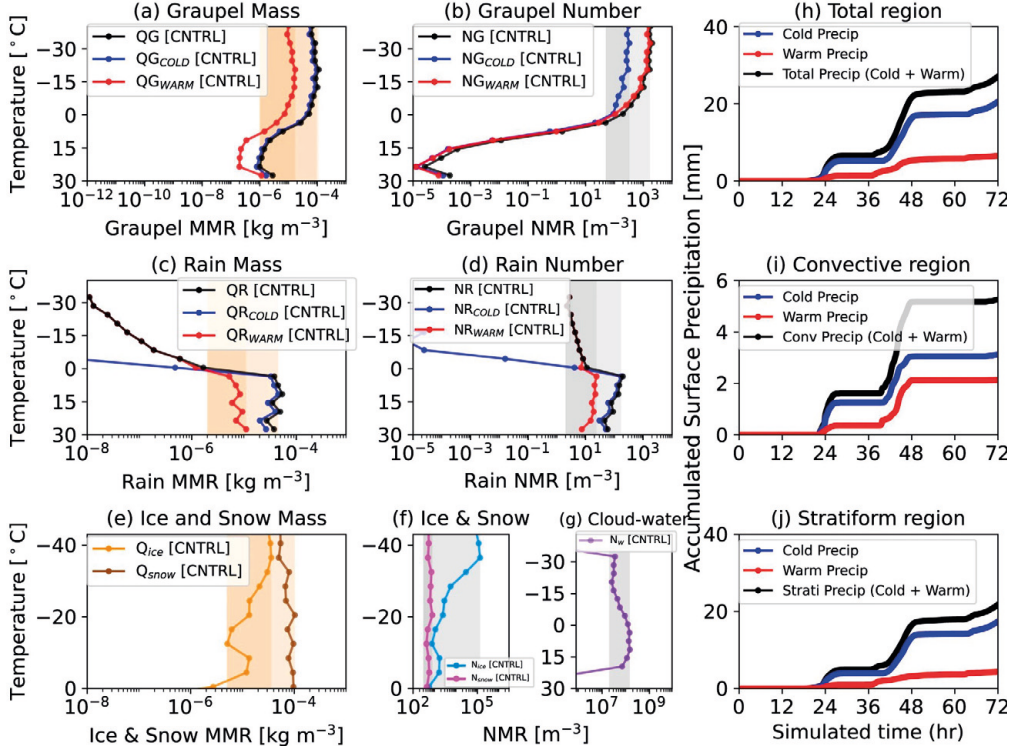


Figure 5.7: Temperature-resolved conditions averaged over cloudy regions of: a mass mixing ratio (MMR) and b number mixing ratio (NMR) of graupel with corresponding warm (red line) and cold (blue line) components; c mass and d number mixing ratios of rain plotted similarly; e ice (orange) and snow (brown) mass mixing ratio; f ice (light blue) and snow (magenta) number mixing ratio; and g cloud water number mixing ratio (purple) for the MC3E case (slightly warm-based convective clouds at 17°C) control simulation using AC during 0000–2300 UTC on 11 May 2011. Also shown is the MC3E case control simulation of the accumulated precipitation (mm) for h the entire domain with all clouds and corresponding components from i convective and j stratiform cloudy (and adjacent clear sky) regions for 72h (10–13 May 2011). The yellow and gray shading boxes in (a–g) are similar to those in Fig. 2, with differences in (b) and (e). b The darkest gray shaded box represents cold rain mass mixing ratio, while medium gray is for warm. e The darkest yellow displays the peak value of ice mass mixing ratio, while medium yellow is for snow. The figure is adapted from Gupta et al. (2023).

4 Implementation of the modified stratiform scheme in SCAM6

SCAM6 was simulated with the stratiform scheme described in the sect.1.2 and convection scheme described in sect. 1.1 for the MC3E storm from 10 May 2011 to 13 May 2011.

Figures 5.8a and b show that the LLS24 scheme shows an increase in the prediction of stratiform precipitation compared to the MG08 scheme. The LLS24 scheme predicts a precipitation rate higher than the observations for both the convective peaks, while the

original unmodified version of the model underpredicts the precipitation.

Figure 5.8 shows that both the original unmodified version of the model and the new scheme have a good agreement of LWC with the aircraft observations. Figure 5.8b shows that the predicted CDNC from the LLS24 run agrees well with the observations at almost all levels.

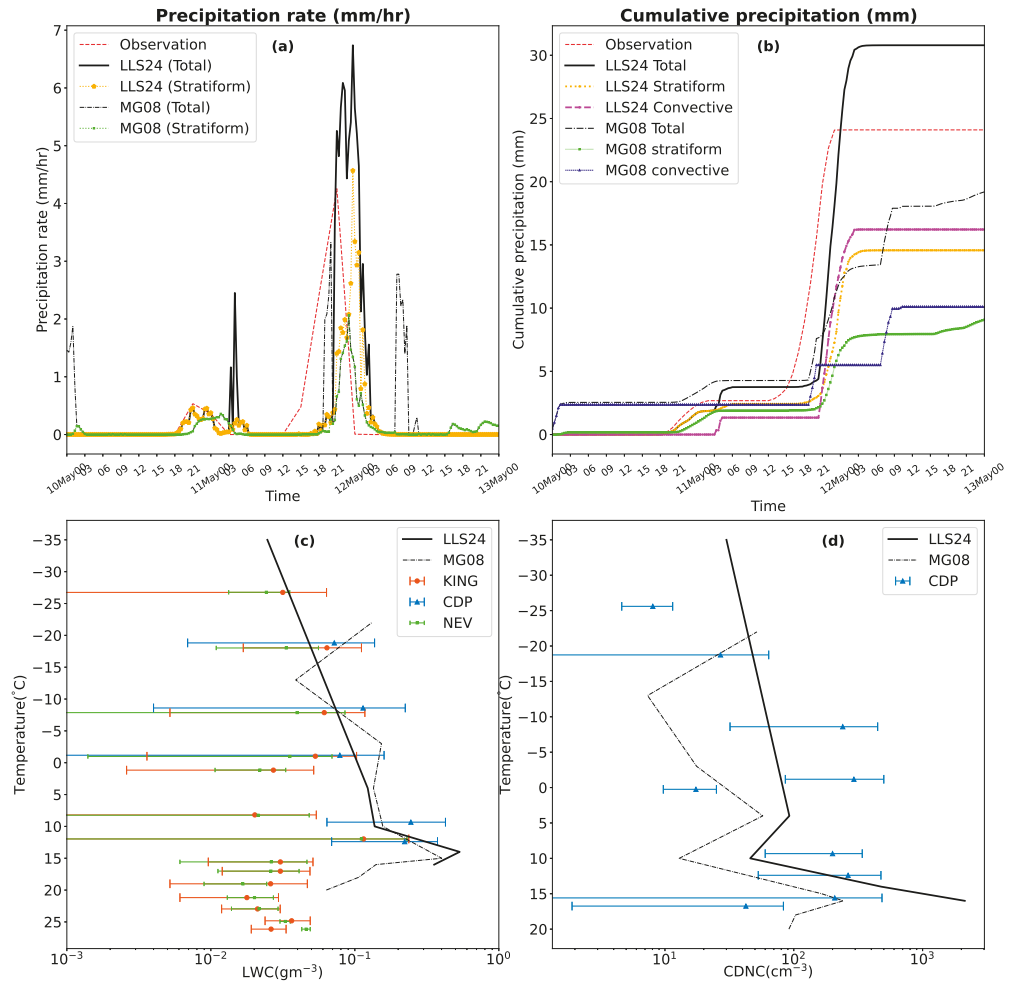


Figure 5.8: Predicted (a) precipitation rate (mm/hr), (b) cumulative surface precipitation, (c) LWC ($g\ m^{-3}$) with CDP, KING and Nevzorov probes, (d) CDNC (cm^{-3}) compared with observations from the CDP probe, from the MG08 (dashdotted black line with square) and LLS24 (solid black line) simulations. Error bars shown are standard errors of observation samples. The cloud microphysical properties are conditionally averaged over the entire simulation period.

The filtered ice concentration plots for the ice particle with sizes greater than 0.2 mm and 1 mm show a good agreement between the predicted values from the LLS24 run.

In figure 5.9d, the ice particle concentrations predicted by the MG08 run are lower than the observations above the freezing levels up to an order of magnitude. Figure 5.9c shows that IWC predicted by the LLS24 run is of the same order of magnitude as the observations below -15°C and shows an error up to 30% above it. MG08 underpredicts the IWC by an order of magnitude at all levels except freezing.

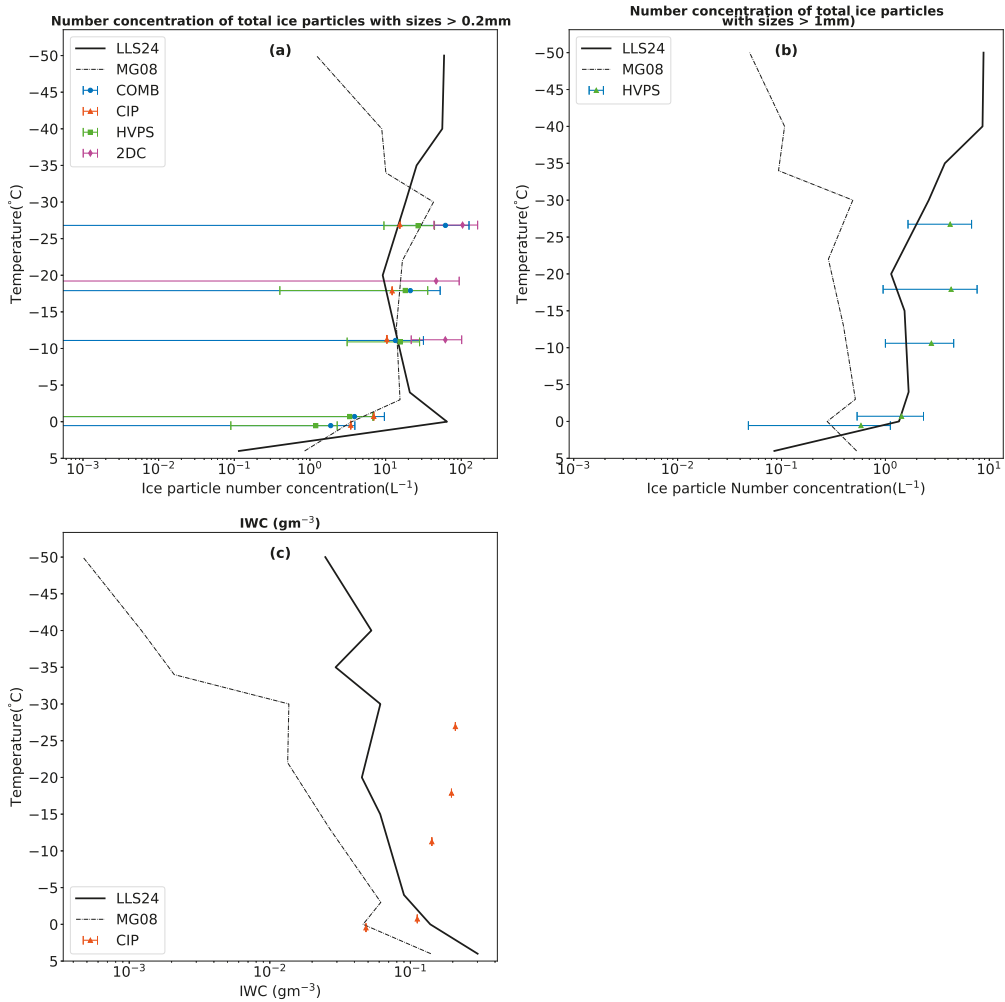


Figure 5.9: Predicted (a) total concentration of ice particles with sizes $> 0.2\text{mm}$ compared with observations from the 2DC, CIP, HVPS-3 probe and COMB, (b) total ice number concentrations of all ice particles with size $> 1\text{mm}$ compared with aircraft observations from the HVPS-3 probe and (c) total IWC from the MG08 (dashed-dotted black line with square) and LLS24 (solid black line) simulations. Error bars shown are standard errors of observation samples.

Chapter 6

Discussions

The research study presented focuses on deep convective cloud parameterisations for a global model, the role of the time dependence of INP activity in initiating ice particles, and the distribution of the warm and cold rain processes in the MC3E storm.

A new deep convective microphysics scheme (ACC scheme) was implemented in the SCAM6. The MC3E storm was simulated with the new convection scheme in the SCAM6, and the results were analysed. AC model studies by Waman et al. (2023) and Gupta et al. (2023) also simulated the MC3E case of 10 May 2011 and the results are discussed here.

The ACC convection scheme is a hybrid bin/bulk microphysics scheme with fine vertical resolution and follows the evolution of the hydrometeor. The ACC scheme shows a good agreement of the cloud microphysical properties with the aircraft observations. The maximum LWC predicted by ACC scheme is 2.6 g m^{-3} . Rosenfeld and Woodley (2000) demonstrated that LWC can reach up to 1.8 gm^{-3} in convective clouds. Prabha et al. (2011) observed LWC between $0.5 - 2 \text{ gm}^{-3}$ for convective clouds during pre-monsoon and monsoon in India. The LWC predicted by the ACC scheme is representative of the convective cloud.

Numerous cloud-modelling studies and measurements have underlined the importance of representation of SIP mechanisms in cloud microphysics to be able to accurately predict the ice particle number concentrations (Mace et al., 2009; Field et al., 2016; Ladino et al., 2017; Sullivan et al., 2017, 2018a; Sotiropoulou et al., 2020, 2021; O’Shea et al., 2021; Atlas et al., 2022). SZ11 microphysics only treats the HM process of rime splintering. Recently Hartmann et al. (2023) did not observe the HM process in their laboratory experiments. Aircraft observations by Harris-Hobbs and Cooper (1987) observed rimed ice in their aircraft observation of warm-based convective clouds. Crosier et al.

(2011) and Lasher-Trapp et al. (2016) observed rimed ice in the regions of the HM process and theorised that the rimed ice was produced from the HM process. The presence of the HM process's existence is uncertain.

In the ACC scheme, the predicted ice concentrations are of the same order of magnitude as the observations. The contribution from the cloud-ice initiated by the three SIP mechanisms are tracked using tagging tracers and have been plotted. Breakup during ice-ice collisions is the most prominent SIP mechanism. In the mixed phase regions, the cloud ice generated from the SIP mechanisms are up to two orders of magnitude higher than the cloud-ice initiated from the heterogeneous ice nucleation. Such high difference in the magnitude would result in the diminishing effect of the heterogeneous ice nucleation in the mixed-phase regions.

The ACC convection scheme predicts a higher precipitation intensity than the observation. The simplified dynamics of considering a single bulk plume do not represent the small-scale dynamic processes in nature, such as overturning and density currents in planetary boundary layer (PBL). The simplified dynamics of the plume do not consider the recirculation of homogeneously nucleated ice into the convective plumes from downdrafts. Another issue in these simulations is that graupel/hail processes are only considered in the ACC scheme. The implementation of a hybrid bin/bulk scheme is more computationally expensive than the original SZ11 scheme. The computation time for the simulations with the ACC scheme was 10 minutes for a single-column model run, whereas SZ11 scheme took only 2 minutes to complete the run.

Deep convective clouds showed a complex response to the changes in the aerosol loading in the environment. In high-CCN run, numerous cloud droplets compete for available water vapour, leading to smaller droplets. Conversely, in the low CCN condition, cloud droplets grow through condensation and effective coalescence, resulting in larger-sized droplets. This is an expected result (Rosenfeld et al., 2008; Andreae and Rosenfeld, 2008; Fan et al., 2016). Above -15°C , the LWC of low-CCN run is higher than the ACC_24 run because of the reduced riming of snow and graupel/hail. Due to the large amount of cloud liquid, there is an increase in freezing of cloud droplets and increased intensity of graupel-snow collisions (Seifert et al., 2012). The increased riming and aggregation in high-CCN, leads to increased concentrations of larger ice particles. In the Low-CCN run because of the large mean cloud droplet diameter the HM process and raindrop freezing fragmentation produce more splinters than the high-CCN run. The changes in the prevailing hydrometeors in different regions of the cloud underline the importance of phase partitioning in clouds.

In high-INP run, the more significant number of initiated cloud droplets leads to reduced collection efficiency and consequently smaller droplet sizes, resulting in decreased rain formation. This increase in LWC for the high-INP occurs due to a de-

creased rate of collision-coalescence among cloud droplets, leading to raindrop formation. In the mixed-phase regions, the number concentration of total ice particles does not show significant change because they are influenced by the intensity of the breakup during ice-ice collisions mechanism.

Role of time-dependent INP freezing in MC3E storm using the SCAM6 and AC simulations. Jakobsson et al. (2022) observed a temperature shift of 0.3 K after 3 minutes of constant isothermal freezing, a weak time dependence. Aerosol samples showed increased INP activity by 70 – 100% when they were isothermally frozen for 2-10 hours. The model simulations of ACC and Waman et al. (2023) predicted a small effect of time-dependent on the overall ice particle concentrations due to the fast convective ascent in the convective regions. The prevalence of the SIP mechanisms in the mixed phase regions is predicted to diminish any small effect by the time-dependence. Both ACC_24 run and simulations by Waman et al. (2023) predict that SIP mechanisms contribute up to 99% of ice particle number concentrations in the mixed phase regions for the MC3E storm.

The precipitation generated by the cold rain and warm rain processes was studied from the simulating the MC3E campaign using the AC model (Gupta et al., 2023). It was predicted that 60% of the total precipitation was from cold precipitation. Gupta et al. (2023) observed that convective precipitation contributed up to 20% to the total accumulated surface precipitation. Whereas the ACC scheme predicts the contribution to be 25%. In the Mc3E case, the cloud droplets were ($\sim 15\mu\text{m}$) smaller than the threshold size ($20 - 25\mu\text{m}$) for coalescence . Additionally, it was predicted that cold precipitation was more by one to two orders of magnitude as compared to warm precipitation.

Chapter 7

Conclusion

The aerosol-cloud interactions are one of the sources of uncertainty in future climate projections (Forster et al., 2021). The impact of aerosols on clouds and the effect of these on the climate system remains uncertain. This includes the impact on the precipitation and the radiative fluxes at different grid-scale (Tao et al., 2012; Boucher et al., 2013; Forster et al., 2021). The large uncertainties arise from the complex nature of the feedback mechanisms and evaluation of physical mechanisms derived from empirical observations and numerical modelling Boucher et al. (2013); Fan et al. (2016). Various studies have revealed different and sometimes contrasting results of the impact of changes in aerosol loading on the deep convective clouds Tao et al. (2012); Fan et al. (2016).

The work presented in this thesis was to improve the aerosol-cloud representation through a detailed hybrid bin/bulk cloud microphysics scheme and also to study the role of various microphysical mechanisms. The conclusions of the study are presented below

1. The validation plots of the convective ACC scheme show an improved estimation of the deep convective cloud properties such as CDNC, LWC, and ice particle number concentrations.
2. The addition of graupel/hail to the microphysics scheme enabled a more realistic representation of the convective clouds' microphysical processes. Results show that graupel/hail and snow mass contribute 96% of the total mass of the ice particles. Snow and graupel/hail have heavy mass and will have higher fall velocities, affecting the precipitation. Gupta et al. (2023) predicted in their high-resolution simulations of the MC3E storm that most of the surface precipitation in the MC3E storm was from cold rain processes. Other studies have also

shown the importance of the representation of graupel/hail in the mesoscale models (Bryan and Morrison, 2012; Van Weverberg, 2013; Wu et al., 2013).

3. The time-dependent INP activity on heterogeneous ice nucleation does not significantly affect the ice particle concentrations in convective clouds. The ascent in the deep-convective clouds is typically a few minutes (5 minutes). Jakobsson et al. (2022) showed a weak time dependence of INP activity at time scales of a few minutes. Waman et al. (2022) showed from their simulations of various cloud types that the effect of time-dependent INP activity $< 10\%$ for deep convective clouds.
4. Simulations from AC model show that time-dependence is not significant in long-lived clouds (Waman et al., 2022) and the persistent ice nucleation was from reactivation and recirculation of dust particles.
5. The SIP mechanisms are prevalent in the mixed-phase regions of the convective clouds and initiate 99% of the ice particle numbers in the mixed-phase areas. For the MC3E storm, it is predicted that fragmentation during ice-ice collisions is the most prolific mechanism, contributing up to 90% of the ice particles in the mixed phase regions. In this storm case, the HM process and raindrop freezing fragmentation are less active because of the smaller size of supercooled drops required for such mechanisms.
6. Sensitivity simulations showed a complex response of convective clouds to the changes in the aerosol loading. Decreasing the aerosol concentrations decreased the accumulated precipitation by 20% from low-CCN to high-CCN. Increasing the CCN concentration resulted in numerous and smaller cloud droplets than in the high-CCN case, which is an expected outcome. These tiny droplets are inefficient in collision coalescence and do not grow by condensation. The richness of supercooled drops in the environment promotes the riming of snow by accretion and increases the activity of the riming of snow in the mixed-phase region.
7. Increasing the INP concentrations increased the cloud-ice initiated from heterogeneous ice nucleation. However, this did not directly increase the ice particle concentrations in the mixed-phase regions. The breakup in ice-ice collisions dampens the effect of the changes in INP on the ice crystal number concentration.
8. In the MC3E storm, most of the precipitation is generated through ice crystal processes. The simulations of the high-resolution AC cloud model by Gupta et al. (2023) demonstrated how fewer INPs lead to reduced snow formation and 60% of the total surface precipitation was generated from cold precipitation.

9. The integration of different SIP mechanisms effectively accounts for the discrepancy between the observed number concentrations of active INPs and total ice particles in simulated clouds.

The analyses in this thesis have raised a new research question regarding the type of parameterisation applied and the study on aerosol-cloud interactions. Conducting sensitivity tests involving microphysical processes such as in-cloud droplet activation and examining the impact of preferential evaporation of supercooled drops at homogeneous freezing levels could offer deeper insight into the observed complex response. The implementation of SBM schemes for microphysical processes resulted in an increased computational time for the model. For bulk cloud microphysics, a single column run took 2 minutes, while with a hybrid bin/bulk scheme, this time was quadrupled. Another approach to enhance representation is through "superparameterisation," where cloud-resolving models are embedded within each grid column of the GCM. These high-resolution 2-D cloud-resolving models simulate cloud processes at a smaller scale, representing the combined effect as heating and cooling rates in the GCMs. Finally, performing the global model simulations with the developed cloud parameterisations for a better representation of aerosol-cloud interactions with the aim of improving climate projections.

1 References

- Albrecht, B. A., 1989: Aerosols, cloud microphysics, and fractional cloudiness. *Science*, **245** (4923), 1227–1230, <https://doi.org/10.1126/SCIENCE.245.4923.1227>.
- Anderson, R. J., R. C. Miller, J. L. Kassner, and D. E. Hagen, 1980: A Study of Homogeneous Condensation-Freezing Nucleation of Small Water Droplets in an Expansion Cloud Chamber. *Journal of Atmospheric Sciences*, **37** (11), 2508 – 2520, [https://doi.org/10.1175/1520-0469\(1980\)037<2508:ASOHCF>2.0.CO;2](https://doi.org/10.1175/1520-0469(1980)037<2508:ASOHCF>2.0.CO;2), URL https://journals.ametsoc.org/view/journals/atsc/37/11/1520-0469_1980_037_2508_asohcf_2_0_co_2.xml.
- Andreae, M. O., and D. Rosenfeld, 2008: Aerosol–cloud–precipitation interactions. Part 1. The nature and sources of cloud-active aerosols. *Earth-Sci.\ Rev.*, **89** (1), 13–41, <https://doi.org/10.1016/j.earscirev.2008.03.001>.
- Arakawa, A., 2004: The Cumulus Parameterization Problem: Past, Present, and Future. *Journal of Climate*, **17** (13), 2493 – 2525, [https://doi.org/10.1175/1520-0442\(2004\)017<2493:RATCPP>2.0.CO;2](https://doi.org/10.1175/1520-0442(2004)017<2493:RATCPP>2.0.CO;2), URL https://journals.ametsoc.org/view/journals/clim/17/13/1520-0442_2004_017_2493_ratcpp_2.0.co_2.xml.

- Atlas, R. L., C. S. Bretherton, M. F. Khairoutdinov, and P. N. Blossey, 2022: Hallett-Mossop Rime Splintering Dims Cumulus Clouds Over the Southern Ocean: New Insight From Nudged Global Storm-Resolving Simulations. *AGU Advances*, **3** (2), e2021AV000454, <https://doi.org/https://doi.org/10.1029/2021AV000454>, URL <https://agupubs.onlinelibrary.wiley.com/doi/abs/10.1029/2021AV000454>.
- Bader, M., J. Gloster, J. L. Brownscombe, and P. Goldsmith, 1974: The production of sub-micron ice fragments by water droplets freezing in free fall or on accretion upon an ice surface. *Quarterly Journal of the Royal Meteorological Society*, **100** (425), 420–426, <https://doi.org/10.1002/QJ.49710042513>, URL <https://onlinelibrary.wiley.com/doi/full/10.1002/qj.49710042513https://onlinelibrary.wiley.com/doi/abs/10.1002/qj.49710042513https://rmets.onlinelibrary.wiley.com/doi/10.1002/qj.49710042513>.
- Bechtold, P., M. Köhler, T. Jung, F. Doblas-Reyes, M. Leutbecher, M. J. Rodwell, F. Vitart, and G. Balsamo, 2008: Advances in simulating atmospheric variability with the ECMWF model: From synoptic to decadal time-scales. *Quarterly Journal of the Royal Meteorological Society*, **134** (634 A), <https://doi.org/10.1002/qj.289>.
- Benmoshe, N., and A. P. Khain, 2014: The effects of turbulence on the microphysics of mixed-phase deep convective clouds investigated with a 2-D cloud model with spectral bin microphysics. *Journal of Geophysical Research: Atmospheres*, **119** (1), 207–221, <https://doi.org/https://doi.org/10.1002/2013JD020118>, URL <https://agupubs.onlinelibrary.wiley.com/doi/abs/10.1002/2013JD020118>.
- Blyth, A. M., and J. Latham, 1993: Development of ice and precipitation in New Mexican summertime cumulus clouds. *Quarterly Journal of the Royal Meteorological Society*, **119** (509), 91–120, <https://doi.org/10.1002/QJ.49711950905>, URL <https://onlinelibrary.wiley.com/doi/full/10.1002/qj.49711950905https://onlinelibrary.wiley.com/doi/abs/10.1002/qj.49711950905https://rmets.onlinelibrary.wiley.com/doi/10.1002/qj.49711950905>.
- Bony, S., and Coauthors, 2015: Clouds, circulation and climate sensitivity. *Nature Geoscience* 2015 8:4, **8** (4), 261–268, <https://doi.org/10.1038/ngeo2398>, URL <https://www.nature.com/articles/ngeo2398>.
- Boucher, O., and Coauthors, 2013: Clouds and Aerosols. *Climate Change 2013: The Physical Science Basis. Contribution of Working Group I to the Fifth Assessment Report of the Intergovernmental Panel on Climate Change*, Cambridge University Press, Cambridge, United Kingdom and New York, NY, USA.
- Bryan, G. H., and H. Morrison, 2012: Sensitivity of a Simulated Squall Line to Horizontal Resolution and Parameterization of Microphysics. *Monthly Weather Review*, **140** (1), 202 – 225, <https://doi.org/https://doi.org/10.1175/MWR-D-11-00046>.

- 1, URL <https://journals.ametsoc.org/view/journals/mwre/140/1/mwr-d-11-00046.1.xml>.
- Cotton, W. R., G. J. Tripoli, R. M. Rauber, and E. A. Mulvihill, 1986: Numerical Simulation of the Effects of Varying Ice Crystal Nucleation Rates and Aggregation Processes on Orographic Snowfall. *Journal of Climate and Applied Meteorology*, **25** (11), 1658–1680, URL <http://www.jstor.org/stable/26183490>.
- Cotton, W. R., and Coauthors, 2003: RAMS 2001: Current status and future directions. *Meteorology and Atmospheric Physics*, **82** (1), 5–29, <https://doi.org/10.1007/s00703-001-0584-9>, URL <https://doi.org/10.1007/s00703-001-0584-9>.
- Crosier, J., and Coauthors, 2011: Observations of ice multiplication in a weakly convective cell embedded in supercooled mid-level stratus. *Atmos. Chem. Phys.*, **11** (1), 257–273, <https://doi.org/10.5194/acp-11-257-2011>.
- Dagan, G., I. Koren, and O. Altaratz, 2015: Aerosol effects on the timing of warm rain processes. *Geophysical Research Letters*, **42** (11), 4590–4598, <https://doi.org/10.1002/2015GL063839>, URL <https://onlinelibrary.wiley.com/doi/full/10.1002/2015GL063839https://onlinelibrary.wiley.com/doi/abs/10.1002/2015GL063839https://agupubs.onlinelibrary.wiley.com/doi/10.1002/2015GL063839>.
- DeMott, P., D. Cziczo, A. Prenni, D. Murphy, S. Kreidenweis, D. Thomson, R. Borys, and D. Rogers, 2003: Measurements of the concentration and composition of nuclei for cirrus formation. *Proc. Natl. Acad. Sci. (USA)*, **100**, 14 655–14 660, <https://doi.org/10.1073/pnas.2532677100>.
- DeMott, P. J., M. P. Meyers, and W. R. Cotton, 1994: Parameterization and Impact of Ice initiation Processes Relevant to Numerical Model Simulations of Cirrus Clouds. *Journal of Atmospheric Sciences*, **51** (1), 77 – 90, [https://doi.org/10.1175/1520-0469\(1994\)051<0077:PAIOII>2.0.CO;2](https://doi.org/10.1175/1520-0469(1994)051<0077:PAIOII>2.0.CO;2), URL https://journals.ametsoc.org/view/journals/atsc/51/1/1520-0469_1994_051_0077_paioui_2_0_co_2.xml.
- Derbyshire, S., A. Maidens, S. Milton, R. Stratton, and M. Willett, 2011: Adaptive detrainment in a convective parametrization. *Quarterly Journal of the Royal Meteorological Society*, **137**, 1856 – 1871, <https://doi.org/10.1002/qj.875>.
- Dong, Y. Y., and J. Hallett, 1989: Droplet accretion during rime growth and the formation of secondary ice crystals. *Quarterly Journal of the Royal Meteorological Society*, **115** (485), 127–142, <https://doi.org/10.1002/QJ.49711548507>, URL <https://onlinelibrary.wiley.com/doi/full/10.1002/qj.49711548507https://onlinelibrary.wiley.com/doi/abs/10.1002/qj.49711548507https://rmets.onlinelibrary.wiley.com/doi/10.1002/qj.49711548507>.

- Doswell, C. A., 2001: Severe Convective Storms—An Overview. *Severe Convective Storms*, C. A. Doswell, Ed., American Meteorological Society, Boston, MA, 1–26, https://doi.org/10.1007/978-1-935704-06-5_{_}1, URL https://doi.org/10.1007/978-1-935704-06-5_1.
- Eytan, E., I. Koren, O. Altaratz, A. B. Kostinski, and A. Ronen, 2020: Long-wave radiative effect of the cloud twilight zone. *Nature Geoscience*, **13** (10), 669–673, <https://doi.org/10.1038/s41561-020-0636-8>, URL <https://doi.org/10.1038/s41561-020-0636-8>.
- Fan, J., Y. Wang, D. Rosenfeld, and X. Liu, 2016: Review of Aerosol–Cloud Interactions: Mechanisms, Significance, and Challenges. *Journal of the Atmospheric Sciences*, **73** (11), 4221–4252, <https://doi.org/10.1175/JAS-D-16-0037.1>, URL <https://journals.ametsoc.org/view/journals/atsc/73/11/jas-d-16-0037.1.xml>.
- Ferrier, B. S., 1994: A Double-Moment Multiple-Phase Four-Class Bulk Ice Scheme. Part I: Description. *J. Atmos. Sci.*, **51** (2), 249 – 280, [https://doi.org/10.1175/1520-0469\(1994\)051<0249:ADMMPF>2.0.CO;2](https://doi.org/10.1175/1520-0469(1994)051<0249:ADMMPF>2.0.CO;2).
- Field, P. R., and A. J. Heymsfield, 2015: Importance of snow to global precipitation. *Geophysical Research Letters*, **42** (21), 9512–9520, <https://doi.org/10.1002/2015GL065497>, URL <https://onlinelibrary.wiley.com/doi/full/10.1002/2015GL065497https://onlinelibrary.wiley.com/doi/abs/10.1002/2015GL065497https://agupubs.onlinelibrary.wiley.com/doi/10.1002/2015GL065497>.
- Field, P. R., A. J. Heymsfield, and A. Bansemer, 2006: Shattering and Particle Interarrival Times Measured by Optical Array Probes in Ice Clouds. *J. Atmos. Oceanic Technol.*, **23** (10), 1357 – 1371, <https://doi.org/10.1175/JTECH1922.1>.
- Field, P. R., and Coauthors, 2016: Chapter 7. Secondary Ice Production - current state of the science and recommendations for the future. *Meteorological Monographs*, <https://doi.org/10.1175/amsmonographs-d-16-0014.1>.
- Findeisen, W., 1938: Kolloid-Meteorologische Vorgänge Bei Niederschlags-Bildung. *Meteor. Z.*, **55**, 121–133.
- Findeisen, W., E. Volken, A. M. Giesche, and S. Brönnimann, 2015: Colloidal meteorological processes in the formation of precipitation. *Meteorologische Zeitschrift*, **24** (4), 443–454, <https://doi.org/10.1127/metz/2015/0675>, URL <http://dx.doi.org/10.1127/metz/2015/0675>.
- Forster, P., and Coauthors, 2021: The Earth’s Energy Budget, Climate Feedbacks, and Climate Sensitivity. *Climate Change 2021: The Physical Science Basis. Contribution of Working Group I to the Sixth Assessment Report of the Intergovernmental*

- Panel on Climate Change*, V. Masson-Delmotte, P. Zhai, A. Pirani, S. L. Connors, C. Péan, S. Berger, N. Caud, Y. Chen, L. Goldfarb, M. I. Gomis, M. Huang, K. Leitzell, E. Lonnoy, J. B. R. Matthews, T. K. Maycock, T. Waterfield, O. Yelekçi, R. Yu, and B. Zhou, Eds., Cambridge University Press, Cambridge, United Kingdom and New York, NY, USA, 923–1054, <https://doi.org/10.1017/9781009157896.009>.
- Gao, W., L. Xue, L. Liu, C. Lu, Y. Yun, and W. Zhou, 2021: A study of the fraction of warm rain in a pre-summer rainfall event over South China. *Atmospheric Research*, **262**, 105–179, <https://doi.org/10.1016/J.ATMOSRES.2021.105792>.
- Gardiner, B. A., and J. Hallett, 1985: Degradation of In-Cloud Forward Scattering Spectrometer Probe Measurements in the Presence of Ice Particles. *Journal of Atmospheric and Oceanic Technology*, **2** (2), [https://doi.org/10.1175/1520-0426\(1985\)002<0171:doicfs>2.0.co;2](https://doi.org/10.1175/1520-0426(1985)002<0171:doicfs>2.0.co;2).
- Gautam Martanda, 2022: Student thesis series INES. Fragmentation in graupel snow collisions. URL <http://lup.lub.lu.se/student-papers/record/9087233>.
- Gettelman, A., M. L. Salby, and F. Sassi, 2002: Distribution and influence of convection in the tropical tropopause region. *Journal of Geophysical Research: Atmospheres*, **107** (D10), 6–1, <https://doi.org/10.1029/2001JD001048>, URL <https://onlinelibrary.wiley.com/doi/full/10.1029/2001JD001048><https://onlinelibrary.wiley.com/doi/abs/10.1029/2001JD001048><https://agupubs.onlinelibrary.wiley.com/doi/10.1029/2001JD001048>.
- Griggs, D. J., and T. W. Chouarton, 1983: Freezing modes of riming droplets with application to ice splinter production. *Quarterly Journal of the Royal Meteorological Society*, **109** (459), 243–253, <https://doi.org/10.1002/QJ.49710945912>, URL <https://onlinelibrary.wiley.com/doi/full/10.1002/qj.49710945912><https://onlinelibrary.wiley.com/doi/abs/10.1002/qj.49710945912><https://rmets.onlinelibrary.wiley.com/doi/10.1002/qj.49710945912>.
- Gupta, A. K., and Coauthors, 2023: The microphysics of the warm-rain and ice crystal processes of precipitation in simulated continental convective storms. *Commun. Earth Environ.*, **4** (1), 226, <https://doi.org/10.1038/s43247-023-00884-5>.
- Hallett, J., and S. C. Mossop, 1974: Production of secondary ice particles during the riming process. *Nature*, **249** (5452), 26–28, <https://doi.org/10.1038/249026a0>.
- Hang, Y., T. S. L'Ecuyer, D. S. Henderson, A. V. Matus, and Z. Wang, 2019: Reassessing the Effect of Cloud Type on Earth's Energy Balance in the Age of Active Spaceborne Observations. Part II: Atmospheric Heating. *Journal of Climate*, **32** (19), 6219–6236, <https://doi.org/10.1175/JCLI-D-18-0754.1>, URL <https://journals.ametsoc.org/view/journals/clim/32/19/jcli-d-18-0754.1.xml>.

- Harris-Hobbs, R. L., and W. A. Cooper, 1987: Field Evidence Supporting Quantitative Predictions of Secondary Ice Production Rates. *J. Atmos. Sci.*, **44** (7), 1071 – 1082, [https://doi.org/10.1175/1520-0469\(1987\)044<1071:FESQPO>2.0.CO;2](https://doi.org/10.1175/1520-0469(1987)044<1071:FESQPO>2.0.CO;2).
- Harrison, E. F., P. Minnis, B. R. Barkstrom, V. Ramanathan, R. D. Cess, and G. G. Gibson, 1990: Seasonal variation of cloud radiative forcing derived from the Earth Radiation Budget Experiment. *Journal of Geophysical Research: Atmospheres*, **95** (D11), 18 687–18 703, <https://doi.org/10.1029/JD095ID11P18687>, URL <https://onlinelibrary.wiley.com/doi/full/10.1029/JD095iD11p18687https://onlinelibrary.wiley.com/doi/abs/10.1029/JD095iD11p18687https://agupubs.onlinelibrary.wiley.com/doi/10.1029/JD095iD11p18687>.
- Hartmann, D. L., M. E. Ockert-Bell, and M. L. Michelsen, 1992: The Effect of Cloud Type on Earth’s Energy Balance: Global Analysis. *Journal of Climate*, **5** (11), 1281 – 1304, [https://doi.org/10.1175/1520-0442\(1992\)005<1281:TEOCTO>2.0.CO;2](https://doi.org/10.1175/1520-0442(1992)005<1281:TEOCTO>2.0.CO;2), URL https://journals.ametsoc.org/view/journals/clim/5/11/1520-0442_1992_005_1281_teocto_2_0_co_2.xml.
- Hartmann, S., J. Seidel, A. Keinert, A. Kiselev, T. Leisner, and F. Stratmann, 2023: Secondary ice production - No evidence of a productive rime-splintering mechanisms during dry and wet growth. *EGU General Assembly 2023*, Vienna, Austria, <https://doi.org/10.5194/egusphere-egu23-11199>.
- Heymsfield, A. J., and M. Hjelmfelt, 1984: Measurements inside Oklahoma thunderstorms during Project SESAME. Tech. Rep. NCAR/TN-230+STR. <https://doi.org/10.5065/D6PZ56SG9>.
- Heymsfield, A. J., L. M. Miloshevich, C. Schmitt, A. Bansemer, C. Twohy, M. R. Poellot, A. Fridlind, and H. Gerber, 2005: Homogeneous Ice Nucleation in Subtropical and Tropical Convection and Its Influence on Cirrus Anvil Microphysics. *J. Atmos. Sci.*, **62** (1), 41 – 64, <https://doi.org/10.1175/JAS-3360.1>.
- Hill, A. A., B. J. Shipway, and I. A. Boutle, 2015: How sensitive are aerosol-precipitation interactions to the warm rain representation? *Journal of Advances in Modeling Earth Systems*, **7** (3), 987–1004, <https://doi.org/10.1002/2014MS000422>, URL <https://onlinelibrary.wiley.com/doi/full/10.1002/2014MS000422https://onlinelibrary.wiley.com/doi/abs/10.1002/2014MS000422https://agupubs.onlinelibrary.wiley.com/doi/10.1002/2014MS000422>.
- Hirst, E., P. H. Kaye, R. S. Greenaway, P. Field, and D. W. Johnson, 2001: Discrimination of micrometre-sized ice and super-cooled droplets in mixed-phase cloud. *Atmospheric Environment*, **35** (1), 33–47, [https://doi.org/10.1016/S1352-2310\(00\)00377-0](https://doi.org/10.1016/S1352-2310(00)00377-0).

- Hobbs, P. V., and R. Farber, 1972: Fragmentation of ice particles in clouds. *Journal de Recherches Atmospheriques*, **6**, 245–258.
- Houze, R. A., 2014: *Cloud Dynamics - Second Edition*, Vol. 104.
- Howard, L., 1803: LXIV. On the modifications of clouds, and on the principles of their production, suspension, and destruction; being the substance of an essay read before the Askesian Society in the session 1802–3. *The Philosophical Magazine*, **16 (64)**, 344–357, <https://doi.org/10.1080/14786440308676358>, URL <https://www.tandfonline.com/doi/abs/10.1080/14786440308676358>.
- Igel, A. L., M. R. Igel, and S. C. van den Heever, 2015: Make It a Double? Sobering Results from Simulations Using Single-Moment Microphysics Schemes. *Journal of the Atmospheric Sciences*, **72 (2)**, 910 – 925, <https://doi.org/10.1175/JAS-D-14-0107.1>, URL <https://journals.ametsoc.org/view/journals/atsc/72/2/jas-d-14-0107.1.xml>.
- Jakobsson, J. K. F., D. B. Waman, V. T. J. Phillips, and T. B. Kristensen, 2022: Time dependence of heterogeneous ice nucleation by ambient aerosols: laboratory observations and a formulation for models. *Atmos. Chem. Phys.*, **22 (10)**, 6717–6748, <https://doi.org/10.5194/acp-22-6717-2022>.
- Jensen, M. P., and Coauthors, 2016: The Midlatitude Continental Convective Clouds Experiment (MC3E). *Bull. Amer. Meteor. Soc.*, **97 (9)**, 1667 – 1686, <https://doi.org/10.1175/BAMS-D-14-00228.1>.
- Johnson, D. A., and J. Hallett, 1968: Freezing and shattering of supercooled water drops. *Quarterly Journal of the Royal Meteorological Society*, **94 (402)**, 468–482, <https://doi.org/https://doi.org/10.1002/qj.49709440204>, URL <https://rmets.onlinelibrary.wiley.com/doi/abs/10.1002/qj.49709440204>.
- Kanji, Z. A., L. A. Ladino, H. Wex, Y. Boose, M. Burkert-Kohn, D. J. Cziczo, and M. Krämer, 2017: Overview of Ice Nucleating Particles. *Meteor. Monogr.*, **58**, 1.1 – 1.33, <https://doi.org/10.1175/AMSMONOGRAPHS-D-16-0006.1>.
- Kessler, E., 1969: On the Distribution and Continuity of Water Substance in Atmospheric Circulations. *On the Distribution and Continuity of Water Substance in Atmospheric Circulations*, 1–84, https://doi.org/10.1007/978-1-935704-36-2_{_}1, URL https://link.springer.com/chapter/10.1007/978-1-935704-36-2_1.
- Khain, A. P., and M. Pinsky, 2018a: Microphysical Processes in Ice and Mixed-Phase Clouds. *Physical Processes in Clouds and Cloud Modeling*, Cambridge University Press, chap. 6, 344–496.

- Khain, A. P., and M. Pinsky, 2018b: *Physical Processes in Clouds and Cloud Modeling*. Cambridge University Press.
- Khain, A. P., and Coauthors, 2015: Representation of microphysical processes in cloud-resolving models: Spectral (bin) microphysics versus bulk parameterization. *Reviews of Geophysics*, **53** (2), 247–322, <https://doi.org/10.1002/2014RG000468>.
- Khairoutdinov, M., and Y. Kogan, 2000: A new cloud physics parameterization in a large-eddy simulation model of marine stratocumulus. *Monthly Weather Review*, **128** (1), [https://doi.org/10.1175/1520-0493\(2000\)128<0229:ANCPPI>2.0.CO;2](https://doi.org/10.1175/1520-0493(2000)128<0229:ANCPPI>2.0.CO;2).
- Kodama, Y. M., M. Katsumata, S. Mori, S. Satoh, Y. Hirose, and H. Ueda, 2009: Climatology of Warm Rain and Associated Latent Heating Derived from TRMM PR Observations. *Journal of Climate*, **22** (18), 4908–4929, <https://doi.org/10.1175/2009JCLI2575.1>, URL <https://journals.ametsoc.org/view/journals/clim/22/18/2009jcli2575.1.xml>.
- Kogan, Y., 2013: A cumulus cloud microphysics parameterization for cloud-resolving models. *Journal of the Atmospheric Sciences*, **70** (5), <https://doi.org/10.1175/JAS-D-12-0183.1>.
- Köhler, H., 1936: The nucleus in and the growth of hygroscopic droplets. *Transactions of the Faraday Society*, **32** (0), 1152–1161, <https://doi.org/10.1039/TF9363201152>, URL <https://pubs.rsc.org/en/content/articlehtml/1936/tf/tf9363201152><https://pubs.rsc.org/en/content/articlelanding/1936/tf/tf9363201152>.
- Kong, F., and M. K. Yau, 1997: An explicit approach to microphysics in MC2. *Atmosphere-Ocean*, **35** (3), 257–291, <https://doi.org/10.1080/07055900.1997.9649594>, URL <https://doi.org/10.1080/07055900.1997.9649594>.
- Korolev, A., and T. Leisner, 2020: Review of experimental studies of secondary ice production. *Atmos.\ Chem.\ Phys.*, **20** (20), 11 767–11 797, <https://doi.org/10.5194/acp-20-11767-2020>.
- Kudzotsa, I., and Coauthors, 2016: Aerosol indirect effects on glaciated clouds. Part I: Model description. *Quarterly Journal of the Royal Meteorological Society*, **142** (698), 1958–1969, <https://doi.org/10.1002/QJ.2791>, URL <https://onlinelibrary.wiley.com/doi/full/10.1002/qj.2791><https://onlinelibrary.wiley.com/doi/abs/10.1002/qj.2791><https://rmets.onlinelibrary.wiley.com/doi/10.1002/qj.2791>.
- Ladino, L. A., A. Korolev, I. Heckman, M. Wolde, A. M. Fridlind, and A. S. Ackerman, 2017: On the role of ice-nucleating aerosol in the formation of ice particles in tropical mesoscale convective systems. *Geophys.\ Res.\ Lett.*, **44** (3), 1574–1582, <https://doi.org/10.1002/2016GL072455>.

- Lamarck, J. B., 1802: Sur la forme des nuages. *Annuaire météorologique pour l'an X de la République française*, **3**, 149–164.
- Lamb, D., and J. Verlinde, 2011: Physics and chemistry of clouds. *Physics and Chemistry of Clouds*, 1–584, <https://doi.org/10.1017/CBO9780511976377>.
- Langmuir, I., 1948: THE PRODUCTION OF RAIN BY A CHAIN REACTION IN CUMULUS CLOUDS AT TEMPERATURES ABOVE FREEZING. *Journal of Atmospheric Sciences*, **5** (5), 175 – 192, [https://doi.org/10.1175/1520-0469\(1948\)005<0175:TPORBA>2.0.CO;2](https://doi.org/10.1175/1520-0469(1948)005<0175:TPORBA>2.0.CO;2), URL https://journals.ametsoc.org/view/journals/atsc/5/5/1520-0469_1948_005_0175_tporba_2_0_co_2.xml.
- Lasher-Trapp, S., D. C. Leon, P. J. DeMott, C. M. Villanueva-Birriel, A. V. Johnson, D. H. Moser, C. S. Tully, and W. Wu, 2016: A multisensor investigation of rime splintering in tropical maritime cumuli. *Journal of the Atmospheric Sciences*, **73** (6), <https://doi.org/10.1175/JAS-D-15-0285.1>.
- Lau, K. M., and H. T. Wu, 2003: Warm rain processes over tropical oceans and climate implications. *Geophysical Research Letters*, **30** (24), 2290, <https://doi.org/10.1029/2003GL018567>, URL <https://onlinelibrary.wiley.com/doi/full/10.1029/2003GL018567https://onlinelibrary.wiley.com/doi/abs/10.1029/2003GL018567https://agupubs.onlinelibrary.wiley.com/doi/10.1029/2003GL018567>.
- Lin, Y.-L., R. D. Farley, and H. D. Orville, 1983: Bulk Parameterization of the Snow Field in a Cloud Model. *J. Climate Appl. Meteor.*, **22** (6), 1065 – 1092, [https://doi.org/10.1175/1520-0450\(1983\)022<1065:BPOTSF>2.0.CO;2](https://doi.org/10.1175/1520-0450(1983)022<1065:BPOTSF>2.0.CO;2).
- Liu, X., and J. E. Penner, 2005: Ice nucleation parameterization for global models. *Meteor. Z.*, **14** (4), 499–514, <https://doi.org/10.1127/0941-2948/2005/0059>.
- Lohmann, U., 2006: Aerosol effects on clouds and climate. *Space Science Reviews*, **125** (1-4), <https://doi.org/10.1007/s11214-006-9051-8>.
- Lohmann, U., F. Lüönd, and F. Mahrt, 2016: *An Introduction to Clouds: From the Microscale to Climate*. Cambridge University Press, Cambridge.
- Mace, G. G., M. Deng, B. Soden, and E. Zipser, 2006: Association of Tropical Cirrus in the 10–15-km Layer with Deep Convective Sources: An Observational Study Combining Millimeter Radar Data and Satellite-Derived Trajectories. *Journal of the Atmospheric Sciences*, **63** (2), 480–503, <https://doi.org/10.1175/JAS3627.1>, URL <https://journals.ametsoc.org/view/journals/atsc/63/2/jas3627.1.xml>.
- Mace, G. G., Q. Zhang, M. Vaughan, R. Marchand, G. Stephens, C. Trepte, and D. Winker, 2009: A description of hydrometeor layer occurrence statistics derived

- from the first year of merged Cloudsat and CALIPSO data. *Journal of Geophysical Research Atmospheres*, **114** (8), <https://doi.org/10.1029/2007JD009755>.
- Mason, B. J., and J. Maybank, 1960: The fragmentation and electrification of freezing water drops. *Quarterly Journal of the Royal Meteorological Society*, **86** (368), 176–185, <https://doi.org/10.1002/QJ.49708636806>, URL <https://onlinelibrary.wiley.com/doi/full/10.1002/qj.49708636806https://onlinelibrary.wiley.com/doi/abs/10.1002/qj.49708636806https://rmets.onlinelibrary.wiley.com/doi/10.1002/qj.49708636806>.
- McFarquhar, G. M., A. J. Heymsfield, J. Spinhirne, and B. Hart, 2000: Thin and Subvisual Tropopause Tropical Cirrus: Observations and Radiative Impacts. *Journal of the Atmospheric Sciences*, **57** (12), 1841 – 1853, [https://doi.org/10.1175/1520-0469\(2000\)057<1841:TASTTC>2.0.CO;2](https://doi.org/10.1175/1520-0469(2000)057<1841:TASTTC>2.0.CO;2), URL https://journals.ametsoc.org/view/journals/atsc/57/12/1520-0469_2000_057_1841_tasttc_2.0.co_2.xml.
- McFarquhar, G. M., H. Zhang, G. Heymsfield, R. Hood, J. Dudhia, J. B. Halverson, and F. Marks, 2006: Factors affecting the evolution of Hurricane Erin (2001) and the distributions of hydrometeors: Role of microphysical processes. *Journal of the Atmospheric Sciences*, **63** (1), 127–150, <https://doi.org/10.1175/JAS3590.1>.
- Meyers, M. P., P. J. Demott, and W. R. Cotton, 1992: New primary ice-nucleation parameterizations in an explicit cloud model. *Journal of Applied Meteorology*, **31** (7), [https://doi.org/10.1175/1520-0450\(1992\)031<0708:NPINPI>2.0.CO;2](https://doi.org/10.1175/1520-0450(1992)031<0708:NPINPI>2.0.CO;2).
- Meyers, M. P., R. L. Walko, J. Y. Harrington, and W. R. Cotton, 1997: New RAMS cloud microphysics parameterization. Part II: The two-moment scheme. *Atmospheric Research*, **45** (1), 3–39, [https://doi.org/10.1016/S0169-8095\(97\)00018-5](https://doi.org/10.1016/S0169-8095(97)00018-5).
- Milbrandt, J. A., and M. K. Yau, 2005a: A multimoment bulk microphysics parameterization. Part I: Analysis of the role of the spectral shape parameter. *Journal of the Atmospheric Sciences*, **62** (9), 3051–3064, <https://doi.org/10.1175/JAS3534.1>.
- Milbrandt, J. A., and M. K. Yau, 2005b: A Multimoment Bulk Microphysics Parameterization. Part II: A Proposed Three-Moment Closure and Scheme Description. *Journal of the Atmospheric Sciences*, **62** (9), 3065–3081, <https://doi.org/10.1175/JAS3535.1>, URL <https://journals.ametsoc.org/view/journals/atsc/62/9/jas3535.1.xml>.
- Ming, Y., V. Ramaswamy, L. J. Donner, and V. T. J. Phillips, 2006: A New Parameterization of Cloud Droplet Activation Applicable to General Circulation Models. *Journal of the Atmospheric Sciences*, **63** (4), 1348–1356, <https://doi.org/10.1175/JAS3686.1>, URL <https://journals.ametsoc.org/view/journals/atsc/63/4/jas3686.1.xml>.

- Morrison, H., J. A. Curry, and V. I. Khvorostyanov, 2005: A new double-moment microphysics parameterization for application in cloud and climate models. Part I: Description. *Journal of the Atmospheric Sciences*, **62** (6), 1665–1677, <https://doi.org/10.1175/JAS3446.1>.
- Morrison, H., and A. Gettelman, 2008: A New Two-Moment Bulk Stratiform Cloud Microphysics Scheme in the Community Atmosphere Model, Version 3 (CAM3). Part I: Description and Numerical Tests. *Journal of Climate*, **21** (15), 3642–3659, <https://doi.org/10.1175/2008JCLI2105.1>, URL <https://journals.ametsoc.org/view/journals/clim/21/15/2008jcli2105.1.xml>.
- O’Shea, S., and Coauthors, 2021: Characterising optical array particle imaging probes: Implications for small-ice-crystal observations. *Atmospheric Measurement Techniques*, **14** (3), <https://doi.org/10.5194/amt-14-1917-2021>.
- Petters, M. D., and S. M. Kreidenweis, 2007: A single parameter representation of hygroscopic growth and cloud condensation nucleus activity. *Atmospheric Chemistry and Physics*, **7** (8), 1961–1971, <https://doi.org/10.5194/ACP-7-1961-2007>.
- Phillips, V. T. J., P. J. DeMott, and C. Andronache, 2008: An empirical parameterization of heterogeneous ice nucleation for multiple chemical species of aerosol. *Journal of the Atmospheric Sciences*, **65** (9), <https://doi.org/10.1175/2007JAS2546.1>.
- Phillips, V. T. J., P. J. Demott, C. Andronache, K. A. Pratt, K. A. Prather, R. Subramanian, and C. Twohy, 2013: Improvements to an Empirical Parameterization of Heterogeneous Ice Nucleation and Its Comparison with Observations. *J. Atmos. Sci.*, **70** (2), 378 – 409, <https://doi.org/10.1175/JAS-D-12-080.1>.
- Phillips, V. T. J., L. J. Donner, and S. T. Garner, 2007: Nucleation Processes in Deep Convection Simulated by a Cloud-System-Resolving Model with Double-Moment Bulk Microphysics. *J. Atmos. Sci.*, **64** (3), 738 – 761, <https://doi.org/10.1175/JAS3869.1>.
- Phillips, V. T. J., M. Formenton, A. Bansemer, I. Kudzotsa, and B. Lienert, 2015: A Parameterization of Sticking Efficiency for Collisions of Snow and Graupel with Ice Crystals: Theory and Comparison with Observations. *Journal of the Atmospheric Sciences*, **72** (12), 4885–4902, <https://doi.org/10.1175/JAS-D-14-0096.1>, URL <https://journals.ametsoc.org/view/journals/atsc/72/12/jas-d-14-0096.1.xml>.
- Phillips, V. T. J., S. Patade, J. Gutierrez, and A. Bansemer, 2018: Secondary Ice Production by Fragmentation of Freezing Drops: Formulation and Theory. *J. Atmos. Sci.*, **75** (9), 3031 – 3070, <https://doi.org/10.1175/JAS-D-17-0190.1>.

- Phillips, V. T. J., J.-I. Yano, and A. Khain, 2017a: Ice Multiplication by Breakup in Ice–Ice Collisions. Part I: Theoretical Formulation. *J. Atmos. Sci.*, **74** (6), 1705 – 1719, <https://doi.org/10.1175/JAS-D-16-0224.1>.
- Phillips, V. T. J., and Coauthors, 2009: Potential impacts from biological aerosols on ensembles of continental clouds simulated numerically. *Biogeosciences*, **6** (6), 987–1014, <https://doi.org/10.5194/bg-6-987-2009>.
- Phillips, V. T. J., and Coauthors, 2017b: Ice Multiplication by Breakup in Ice–Ice Collisions. Part II: Numerical Simulations. *J. Atmos. Sci.*, **74** (9), 2789 – 2811, <https://doi.org/10.1175/JAS-D-16-0223.1>.
- Phillips, V. T. J., and Coauthors, 2020: Multiple Environmental Influences on the Lightning of Cold-Based Continental Cumulonimbus Clouds. Part I: Description and Validation of Model. *J. Atmos. Sci.*, **77** (12), 3999 – 4024, <https://doi.org/10.1175/JAS-D-19-0200.1>.
- Prabha, T. V., A. Khain, R. S. Maheshkumar, G. Pandithurai, J. R. Kulkarni, M. Konwar, and B. N. Goswami, 2011: Microphysics of Premonsoon and Monsoon Clouds as seen from In Situ Measurements during the Cloud Aerosol Interaction and Precipitation Enhancement Experiment (CAIPEEX). *J. Atmos. Sci.*, **68** (9), 1882 – 1901, <https://doi.org/10.1175/2011JAS3707.1>.
- Pringle, K. J., H. Tost, A. Pozzer, U. Pöschl, and J. Lelieveld, 2010: Global distribution of the effective aerosol hygroscopicity parameter for CCN activation. *Atmospheric Chemistry and Physics*, **10** (12), 5241–5255, <https://doi.org/10.5194/ACP-10-5241-2010>.
- Pruppacher, H. R., 1967: On the growth of ice crystals in supercooled water and aqueous solution drops. *Pure and Applied Geophysics PAGEOPH*, **68** (1), 186–195, <https://doi.org/10.1007/BF00874894>, URL <https://link.springer.com/article/10.1007/BF00874894>.
- Pruppacher, H. R., and J. D. Klett, 2010: *Microphysics of Clouds and Precipitation*, Atmospheric and Oceanographic Sciences Library, Vol. 18. Springer Dordrecht, <https://doi.org/10.1007/978-0-306-48100-0>.
- Pruppacher, H. R., and R. J. Schlamp, 1975: A wind tunnel investigation on ice multiplication by freezing of waterdrops falling at terminal velocity in air. *Journal of Geophysical Research*, **80** (3), 380–386, <https://doi.org/10.1029/JC080I003P00380>, URL <https://onlinelibrary.wiley.com/doi/full/10.1029/JC080i003p00380><https://onlinelibrary.wiley.com/doi/abs/10.1029/JC080i003p00380><https://agupubs.onlinelibrary.wiley.com/doi/10.1029/JC080i003p00380>.

- Qin, F., and Y. Fu, 2016: TRMM-observed summer warm rain over the tropical and subtropical Pacific Ocean: Characteristics and regional differences. *Journal of Meteorological Research*, **30** (3), 371–385, <https://doi.org/10.1007/S13351-016-5151-X/METRICS>, URL <https://link.springer.com/article/10.1007/s13351-016-5151-x>.
- Qu, Y., A. Khain, V. Phillips, E. Ilotoviz, J. Shpund, S. Patade, and B. Chen, 2020: The Role of Ice Splintering on Microphysics of Deep Convective Clouds Forming Under Different Aerosol Conditions: Simulations Using the Model With Spectral Bin Microphysics. *Journal of Geophysical Research: Atmospheres*, **125** (3), <https://doi.org/10.1029/2019JD031312>.
- Rangno, A. L., and P. V. Hobbs, 2001: Ice particles in stratiform clouds in the Arctic and possible mechanisms for the production of high ice concentrations. *Journal of Geophysical Research: Atmospheres*, **106** (D14), 15 065–15 075, <https://doi.org/10.1029/2000JD900286>, URL <https://onlinelibrary.wiley.com/doi/full/10.1029/2000JD900286><https://onlinelibrary.wiley.com/doi/abs/10.1029/2000JD900286><https://agupubs.onlinelibrary.wiley.com/doi/10.1029/2000JD900286>.
- Rio, C., A. D. Del Genio, and F. Hourdin, 2019: Ongoing Breakthroughs in Convective Parameterization. *Current Climate Change Reports 2019 5:2*, **5** (2), 95–111, <https://doi.org/10.1007/S40641-019-00127-W>, URL <https://link.springer.com/article/10.1007/s40641-019-00127-w>.
- Rogers, R. R., and M. K. Yau, 1989: *A Short Course in Cloud Physics*. 3rd ed., Elsevier, 304 pp.
- Rogers, R. R., and M. K. Yau, 1996: *A First Course in Cloud Physics*.
- Rosenfeld, D., U. Lohmann, G. B. Raga, C. D. O’Dowd, M. Kulmala, S. Fuzzi, A. Reissell, and M. O. Andreae, 2008: Flood or drought: How do aerosols affect precipitation? *Science*, **321** (5894), 1309–1313, https://doi.org/10.1126/SCIENCE.1160606/ASSET/869957B9-D753-42D3-97F0-D04B2213BDC1/ASSETS/GRAPHIC/321{_}1309{_}F4.JPEG, URL <https://www.science.org/doi/10.1126/science.1160606>.
- Rosenfeld, D., and W. L. Woodley, 2000: Deep convective clouds with sustained supercooled liquid water down to - 37.5 °C. *Nature*, **405** (6785), 440–442, <https://doi.org/10.1038/35013030>.
- Saleeby, S. M., and W. R. Cotton, 2004: A Large-Droplet Mode and Prognostic Number Concentration of Cloud Droplets in the Colorado State University Regional Atmospheric Modeling System (RAMS). Part I: Module Descriptions and Supercell Test Simulations. *Journal of Applied Meteorology*,

- 43 (1)**, 182 – 195, [https://doi.org/10.1175/1520-0450\(2004\)043<0182:ALMAPN>2.0.CO;2](https://doi.org/10.1175/1520-0450(2004)043<0182:ALMAPN>2.0.CO;2), URL https://journals.ametsoc.org/view/journals/apme/43/1/1520-0450_2004_043_0182_almapn_2.0.co_2.xml.
- Sassen, K., Z. Wang, and D. Liu, 2008: Global distribution of cirrus clouds from CloudSat/Cloud-Aerosol Lidar and Infrared Pathfinder Satellite Observations (CALIPSO) measurements. *Journal of Geophysical Research: Atmospheres*, **113 (D8)**, 0–12, <https://doi.org/10.1029/2008JD009972>, URL <https://onlinelibrary.wiley.com/doi/full/10.1029/2008JD009972https://onlinelibrary.wiley.com/doi/abs/10.1029/2008JD009972https://agupubs.onlinelibrary.wiley.com/doi/10.1029/2008JD009972>.
- Schoenberg Ferrier, B., 1994: A Double-Moment Multiple-Phase Four-Class Bulk Ice Scheme. Part I: Description. *Journal of the Atmospheric Sciences*, **51 (2)**, 249–280, [https://doi.org/https://doi.org/10.1175/1520-0469\(1994\)051<0249:ADMMPF>2.0.CO;2](https://doi.org/https://doi.org/10.1175/1520-0469(1994)051<0249:ADMMPF>2.0.CO;2), URL [http://journals.ametsoc.org/doi/10.1175/1520-0469\(1994\)051<0249:ADMMPF>2.0.CO;2](http://journals.ametsoc.org/doi/10.1175/1520-0469(1994)051<0249:ADMMPF>2.0.CO;2).
- Schwarzenboeck, A., V. Shcherbakov, R. Lefevre, J.-F. Gayet, Y. Pointin, and C. Duroure, 2009: Indications for stellar-crystal fragmentation in Arctic clouds. *Atmospheric Research*, **92 (2)**, 220–228, <https://doi.org/https://doi.org/10.1016/j.atmosres.2008.10.002>, URL <https://www.sciencedirect.com/science/article/pii/S0169809508002792>.
- Seifert, A., and K. D. Beheng, 2001: A double-moment parameterization for simulating autoconversion, accretion and selfcollection. *Atmospheric Research*, **59-60**, 265–281, [https://doi.org/10.1016/S0169-8095\(01\)00126-0](https://doi.org/10.1016/S0169-8095(01)00126-0).
- Seifert, A., C. Köhler, and K. D. Beheng, 2012: Aerosol-cloud-precipitation effects over Germany as simulated by a convective-scale numerical weather prediction model. *Atmos. Chem. Phys.*, **12**, 709–725, <https://doi.org/10.5194/acp-12-709-2012>, URL www.atmos-chem-phys.net/12/709/2012/.
- Seifert, A., L. Nuijens, and B. Stevens, 2010: Turbulence effects on warm-rain autoconversion in precipitating shallow }convection. *QUARTERLY JOURNAL OF THE ROYAL METEOROLOGICAL SOCIETY*, **136 (652, A)**, 1753–1762, <https://doi.org/10.1002/qj.684>.
- Sherwood, S. C., and Coauthors, 2020: An Assessment of Earth’s Climate Sensitivity Using Multiple Lines of Evidence. *Reviews of Geophysics*, **58 (4)**, e2019RG000678, <https://doi.org/10.1029/2019RG000678>, URL <https://onlinelibrary.wiley.com/doi/full/10.1029/2019RG000678https://onlinelibrary.wiley.com/doi/abs/10.1029/2019RG000678https://agupubs.onlinelibrary.wiley.com/doi/10.1029/2019RG000678>.

- Simpson, J., and V. Wiggert, 1969: Models of precipitating cumulus towers. *Monthly Weather Review*, **97** (7), [https://doi.org/10.1175/1520-0493\(1969\)097<0471:mopct>2.3.co;2](https://doi.org/10.1175/1520-0493(1969)097<0471:mopct>2.3.co;2).
- Smull, B. F., 1995: Convectively induced mesoscale weather systems in the tropical and warm-season midlatitude atmosphere. *Reviews of Geophysics*, **33** (S2), 897–906, <https://doi.org/10.1029/95RG00339>, URL <https://onlinelibrary.wiley.com/doi/full/10.1029/95RG00339https://onlinelibrary.wiley.com/doi/abs/10.1029/95RG00339https://agupubs.onlinelibrary.wiley.com/doi/10.1029/95RG00339>.
- Song, X., and G. J. Zhang, 2011: Microphysics parameterization for convective clouds in a global climate model: Description and single-column model tests. *J. Geophys. Res. Atmos.*, **116** (D2), <https://doi.org/10.1029/2010JD014833>.
- Sotiropoulou, G., S. Sullivan, J. Savre, G. Lloyd, T. Lachlan-Cope, A. M. L. Ekman, and A. Nenes, 2020: The impact of secondary ice production on Arctic stratocumulus. *Atmos. Chem. Phys.*, **20** (3), 1301–1316, <https://doi.org/10.5194/acp-20-1301-2020>, URL <https://acp.copernicus.org/articles/20/1301/2020/>.
- Sotiropoulou, G., Vignon, G. Young, H. Morrison, S. J. O’Shea, T. Lachlan-Cope, A. Berne, and A. Nenes, 2021: Secondary ice production in summer clouds over the Antarctic coast: }an underappreciated process in atmospheric models. *Atmospheric Chemistry and Physics*, **21** (2), 755–771, <https://doi.org/10.5194/acp-21-755-2021>.
- Stevens, B., and G. Feingold, 2009: Untangling aerosol effects on clouds and precipitation in a buffered system. *Nature* 2009 461:7264, **461** (7264), 607–613, <https://doi.org/10.1038/nature08281>, URL <https://www.nature.com/articles/nature08281>.
- Storelvmo, T., and I. Tan, 2015: The Wegener-Bergeron-Findeisen process ? Its discovery and vital importance for weather and climate. *Meteorologische Zeitschrift*, **24** (4), 455–461, <https://doi.org/10.1127/metz/2015/0626>, URL <http://dx.doi.org/10.1127/metz/2015/0626>.
- Stubenrauch, C. J., and Coauthors, 2013: Assessment of global cloud datasets from satellites: Project and database initiated by the GEWEX radiation panel. *Bulletin of the American Meteorological Society*, **94** (7), <https://doi.org/10.1175/BAMS-D-12-00117.1>.
- Sullivan, S. C., C. Barthlott, J. Crosier, I. Zhukov, A. Nenes, and C. Hoose, 2018a: The effect of secondary ice production parameterization on the simulation of a cold frontal rainband. *Atmos. Chem. Phys.*, **18** (22), 16 461–16 480, <https://doi.org/10.5194/acp-18-16461-2018>, URL <https://acp.copernicus.org/articles/18/16461/2018/>.

- Sullivan, S. C., C. Hoose, A. Kiselev, T. Leisner, and A. Nenes, 2018b: Initiation of secondary ice production in clouds. *Atmos. Chem. Phys.*, **18** (3), 1593–1610, <https://doi.org/10.5194/acp-18-1593-2018>, URL <https://acp.copernicus.org/articles/18/1593/2018/>.
- Sullivan, S. C., C. Hoose, and A. Nenes, 2017: Investigating the contribution of secondary ice production to in-cloud ice crystal numbers. *J. Geophys. Res. Atmos.*, **122** (17), 9391–9412, <https://doi.org/10.1002/2017JD026546>.
- Takahashi, T., Y. Nagao, and Y. Kushiyama, 1995: Possible High Ice Particle Production during Graupel–Graupel Collisions. *J. Atmos. Sci.*, **52** (24), 4523 – 4527, [https://doi.org/10.1175/1520-0469\(1995\)052<4523:PHIPPD>2.0.CO;2](https://doi.org/10.1175/1520-0469(1995)052<4523:PHIPPD>2.0.CO;2).
- Takemura, T., 2012: Distributions and climate effects of atmospheric aerosols from the preindustrial era to 2100 along Representative Concentration Pathways (RCPs) simulated using the global aerosol model SPRINTARS. *Atmospheric Chemistry and Physics*, **12** (23), 11 555–11 572, <https://doi.org/10.5194/ACP-12-11555-2012>.
- Tan, I., T. Storelvmo, and M. D. Zelinka, 2018: The Climatic Impact of Thermodynamic Phase Partitioning in Mixed-Phase Clouds. *Mixed-Phase Clouds: Observations and Modeling*, 237–264, <https://doi.org/10.1016/B978-0-12-810549-8.00010-6>.
- Tao, W. K., J. P. Chen, Z. Li, C. Wang, and C. Zhang, 2012: Impact of aerosols on convective clouds and precipitation. *Reviews of Geophysics*, **50** (2), 2001, <https://doi.org/10.1029/2011RG000369>, URL <https://onlinelibrary.wiley.com/doi/full/10.1029/2011RG000369><https://onlinelibrary.wiley.com/doi/abs/10.1029/2011RG000369><https://agupubs.onlinelibrary.wiley.com/doi/10.1029/2011RG000369>.
- Tao, W.-K., and J. Simpson, 1993: Goddard cumulus ensemble model. Part I: Model description. *Terr. Atmos. Ocean. Sci.*, **4** (1), 35–72.
- Tory, K. J., M. T. Montgomery, and N. E. Davidson, 2006: Prediction and Diagnosis of Tropical Cyclone Formation in an NWP System. Part I: The Critical Role of Vortex Enhancement in Deep Convection. *Journal of the Atmospheric Sciences*, **63** (12), 3077–3090, <https://doi.org/10.1175/JAS3764.1>, URL <https://journals.ametsoc.org/view/journals/atsc/63/12/jas3764.1.xml>.
- Twomey, S., 1974: Pollution and the planetary albedo. *Atmos. Environ.*, **8** (12), 1251–1256, [https://doi.org/10.1016/0004-6981\(74\)90004-3](https://doi.org/10.1016/0004-6981(74)90004-3).
- Twomey, S., 1977: The Influence of Pollution on the Shortwave Albedo of Clouds. *J. Atmos. Sci.*, **34** (7), 1149 – 1152, [https://doi.org/10.1175/1520-0469\(1977\)034<1149:TIOPOP>2.0.CO;2](https://doi.org/10.1175/1520-0469(1977)034<1149:TIOPOP>2.0.CO;2).

- Vali, G., 1996: Ice Nucleation — a review. *Nucleation and Atmospheric Aerosols 1996*, 271–279, <https://doi.org/10.1016/B978-008042030-1/50066-4>.
- Vali, G., 1999: Ice nucleation-theory: a tutorial. *NCAR/ASP 1999 Summer Colloquium*, 599.
- Vali, G., P. J. Demott, O. Möhler, and T. F. Whale, 2015: Technical Note: A proposal for ice nucleation terminology. *Atmos. Chem. Phys.*, **15**, 10 263–10 270, <https://doi.org/10.5194/acp-15-10263-2015>, URL www.atmos-chem-phys.net/15/10263/2015/.
- Van Weverberg, K., 2013: Impact of environmental instability on convective precipitation uncertainty associated with the nature of the rimed ice species in a bulk microphysics scheme. *Monthly Weather Review*, **141** (8), 2841–2849, <https://doi.org/10.1175/MWR-D-13-00036.1>.
- Vardiman, L., 1978: The Generation of Secondary Ice Particles in Clouds by Crystal–Crystal Collision. *Journal of the Atmospheric Sciences*, **35** (11), [https://doi.org/10.1175/1520-0469\(1978\)035<2168:tgosip>2.0.co;2](https://doi.org/10.1175/1520-0469(1978)035<2168:tgosip>2.0.co;2).
- Walko, R. L., W. R. Cotton, M. P. Meyers, and J. Y. Harrington, 1995: New RAMS cloud microphysics parameterization part I: the single-moment scheme. *Atmospheric Research*, **38** (1-4), 29–62, [https://doi.org/10.1016/0169-8095\(94\)00087-T](https://doi.org/10.1016/0169-8095(94)00087-T).
- Waman, D., A. Deshmukh, A. Jadav, S. Patade, M. Gautam, V. Phillips, A. Bansemer, and J. Jakobsson, 2023: Effects from time dependence of ice nucleus activity for contrasting cloud types. *Journal of the Atmospheric Sciences*, <https://doi.org/10.1175/JAS-D-22-0187.1>, URL <https://journals.ametsoc.org/view/journals/atsc/aop/JAS-D-22-0187.1/JAS-D-22-0187.1.xml>.
- Waman, D., S. Patade, A. Jadav, A. Deshmukh, A. K. Gupta, V. T. J. Phillips, A. Bansemer, and P. J. DeMott, 2022: Dependencies of Four Mechanisms of Secondary Ice Production on Cloud-Top Temperature in a Continental Convective Storm. *Journal of the Atmospheric Sciences*, **79** (12), 3375 – 3404, <https://doi.org/10.1175/JAS-D-21-0278.1>, URL <https://journals.ametsoc.org/view/journals/atsc/79/12/JAS-D-21-0278.1.xml>.
- Wang, C., and J. S. Chang, 1993: A three-dimensional numerical model of cloud dynamics, microphysics, and chemistry: 1. Concepts and formulation. *Journal of Geophysical Research: Atmospheres*, **98** (D8), 14 827–14 844, <https://doi.org/10.1029/92JD01393>, URL <https://onlinelibrary.wiley.com/doi/full/10.1029/92JD01393><https://onlinelibrary.wiley.com/doi/abs/10.1029/92JD01393><https://agupubs.onlinelibrary.wiley.com/doi/10.1029/92JD01393>.

- Wegener, A., 1912: Thermodynamik der Atmosphäre. *Nature*, **90** (2237), 31, <https://doi.org/10.1038/090031a0>, URL <https://doi.org/10.1038/090031a0>.
- Wood, R., 2012: Stratocumulus Clouds. *Monthly Weather Review*, **140** (8), 2373–2423, <https://doi.org/10.1175/MWR-D-11-00121.1>, URL <https://journals.ametsoc.org/view/journals/mwre/140/8/mwr-d-11-00121.1.xml>.
- Wood, R., 2015: CLOUDS AND FOG | Stratus and Stratocumulus. *Encyclopedia of Atmospheric Sciences: Second Edition*, 196–200, <https://doi.org/10.1016/B978-0-12-382225-3.00396-0>.
- Wu, D., X. Dong, B. Xi, Z. Feng, A. Kennedy, G. Mullendore, M. Gilmore, and W.-K. Tao, 2013: Impacts of microphysical scheme on convective and stratiform characteristics in two high precipitation squall line events. *J. Geophys. Res. Atmos.*, **118** (19), 111–119, <https://doi.org/10.1002/jgrd.50798>.
- Xie, S., Y. Zhang, S. E. Giangrande, M. P. Jensen, R. McCoy, and M. Zhang, 2014: Interactions between cumulus convection and its environment as revealed by the MC3E sounding array. *J. Geophys. Res. Atmos.*, **119** (20), 711–784, <https://doi.org/10.1002/2014JD022011>.
- Yang, J., Z. Wang, A. J. Heymsfield, and J. R. French, 2016: Characteristics of vertical air motion in isolated convective clouds. *Atmospheric Chemistry and Physics*, **16** (15), 10 159–10 173, <https://doi.org/10.5194/ACP-16-10159-2016>.
- Yano, J. I., V. T. Phillips, and V. Kanawade, 2016: Explosive ice multiplication by mechanical break-up in ice–ice collisions: a dynamical system-based study. *Quarterly Journal of the Royal Meteorological Society*, **142** (695), 867–879, <https://doi.org/10.1002/QJ.2687>, URL <https://onlinelibrary.wiley.com/doi/full/10.1002/qj.2687https://onlinelibrary.wiley.com/doi/abs/10.1002/qj.2687https://rmets.onlinelibrary.wiley.com/doi/10.1002/qj.2687>.
- Yano, J.-I., and V. T. J. Phillips, 2011: Ice–Ice Collisions: An Ice Multiplication Process in Atmospheric Clouds. *J. Atmos. Sci.*, **68** (2), 322 – 333, <https://doi.org/10.1175/2010JAS3607.1>.
- Zelinka, M. D., I. Tan, L. Oreopoulos, and G. Tselioudis, 2023: Detailing cloud property feedbacks with a regime-based decomposition. *Climate Dynamics*, **60** (9–10), 2983–3003, <https://doi.org/10.1007/S00382-022-06488-7/FIGURES/11>, URL <https://link.springer.com/article/10.1007/s00382-022-06488-7>.
- Zhang, G. J., and N. A. McFarlane, 1995: Sensitivity of climate simulations to the parameterization of cumulus convection in the Canadian climate centre general circulation model. *Atmos.–Ocean*, **33** (3), 407–446, <https://doi.org/10.1080/07055900.1995.9649539>.

Ziegler, C. L., 1985: Retrieval of Thermal and Microphysical Variables in Observed Convective Storms. Part 1: Model Development and Preliminary Testing. *Journal of Atmospheric Sciences*, **42** (14), 1487 – 1509, [https://doi.org/10.1175/1520-0469\(1985\)042<1487:ROTAMV>2.0.CO;2](https://doi.org/10.1175/1520-0469(1985)042<1487:ROTAMV>2.0.CO;2), URL https://journals.ametsoc.org/view/journals/atsc/42/14/1520-0469_1985_042_1487_rotamv_2_0_co_2.xml.

